

To appear in ...

Spectral classification and properties of the O Vz stars in the Galactic O-Star Spectroscopic Survey (GOSSS)

Julia I. Arias¹

Departamento de Física y Astronomía, Universidad de La Serena, Chile

`jarias@userena.cl`

Nolan R. Walborn²

Sergio Simón Díaz³

Rodolfo H. Barbá¹

Jesús Maíz Apellániz⁴

Carolina Sabín-Sanjulián¹

Roberto C. Gamen⁵

Nidia I. Morrell⁶

Alfredo Sota⁷

Amparo Marco^{8,9}

Ignacio Negueruela⁸

João R. S. Leão¹⁰

Artemio Herrero³

and

Emilio J. Alfaro⁷

ABSTRACT

On the basis of the Galactic O-Star Spectroscopic Survey (GOSSS), a detailed systematic investigation of the O V_z stars is presented. The currently used spectral classification criteria are rediscussed, and the V_z phenomenon is recalibrated through the addition of a quantitative criterion based on the equivalent widths of the He I $\lambda 4471$, He II $\lambda 4542$, and He II $\lambda 4686$ spectral lines. The GOSSS O V_z and O V populations resulting from the newly adopted spectral classification criteria are comparatively analyzed. The locations of the O V_z stars are probed, showing a concentration of the most extreme cases toward the youngest star forming regions. The occurrence of the V_z spectral peculiarity in a solar-metallicity environment, as predicted by the FASTWIND code, is also investigated, confirming the importance of taking into account several processes for the correct interpretation of the phenomenon.

Subject headings: stars: early-type — stars: fundamental parameters — surveys

¹Departamento de Física y Astronomía, Universidad de La Serena, Av. Cisternas 1200 Norte, La Serena, Chile

²Space Telescope Science Institute, 3700 San Martin Drive, MD 21218, Baltimore, USA

³Instituto de Astrofísica de Canarias, E-38200, Departamento de Astrofísica, Universidad de La Laguna, E-38205, La Laguna, Tenerife, Spain

⁴Centro de Astrobiología, CSIC-INTA, campus ESAC, Camino Bajo del Castillo s/n, E-28 692 Madrid, Spain

⁵Instituto de Astrofísica de La Plata (CONICET, UNLP), Facultad de Ciencias Astronómicas y Geofísicas, Universidad Nacional de La Plata, Paseo del Bosque s/n, 1900 La Plata, Argentina

⁶Las Campanas Observatory, Carnegie Observatories, Casilla 601, La Serena, Chile

⁷Instituto de Astrofísica de Andalucía-CSIC, Glorieta de la Astronomía s/n, E-18 008 Granada, Spain

⁸Departamento de Física, Ingeniería de Sistemas y Teoría de la Señal, Escuela Politécnica Superior, Universidad de Alicante, Carretera San Vicente del Raspeig s/n, E03690, San Vicente del Raspeig, Spain

⁹Department of Astronomy, University of Florida, 211 Bryant Space Science Center, Gainesville, FL 32611

¹⁰Universidade Federal do Rio Grande do Norte - UFRN Caixa Postal 1524 - Campus Universitário Lagoa Nova, CEP 59078-970 — Natal/RN - Brasil

1. Introduction

Walborn (1973) first noted that the spectra of some O dwarfs in the very young Galactic cluster Trumpler 14 in the Carina Nebula showed the He II $\lambda 4686$ absorption substantially stronger, relative to the other He lines, than observed in typical class V spectra. After that, more extreme examples of objects showing this peculiarity were found in the Large Magellanic Cloud (LMC), in particular, in the extremely young star-forming regions N11 (Walborn & Parker 1992, Parker et al. 1992) and 30 Doradus (Walborn & Blades 1997). These discoveries led to the introduction, in the latter paper, of a new luminosity subclass named Vz, “z” chosen for Zero Age Main Sequence (ZAMS), as this characteristic was hypothesized to be a signature of youth.

The idea behind the hypothesis that relates the Vz phenomenon to the small age of the object is that it represents an “inverse” behaviour of the selective emission effect observed among O stars, the Of phenomenon, which is due to the emission filling of the He II $\lambda 4686$ line and correlates with increasing luminosity (Walborn 2001). In other words, the typical class V spectra would already have some emission filling in the He II $\lambda 4686$ line, whereas the Vz objects would have less, thus being less luminous and less evolved, i.e. they would be closer to the ZAMS.

Over the last decades, numerous examples of objects belonging to the OVz class have been identified, both in the Galaxy and the Magellanic Clouds. Walborn (2009) presented a compilation of 50 optically observable ZAMS O candidates that included several stars classified as OVz. In spite of their probable key role for understanding the early evolution of massive stars, quantitative studies of individual OVz stars have been very scarce for years. Moreover, some of these isolated studies place the Vz objects on, while others locate them departed from, the ZAMS, which has provoked some controversy regarding whether or not the Vz spectroscopic classification implies extreme youth.

Very recently the number of known OVz stars in the LMC was significantly increased thanks to the VLT-FLAMES Tarantula Survey (VFTS) ESO Large Programme (Evans et al. 2011). Its huge spectroscopic dataset permitted the detection of no fewer than 48 OVz objects among a sample of 213 O stars in the 30 Doradus region (Walborn et al. 2014). Sabín-Sanjulián et al. (2014; hereafter SS14) took advantage of this dataset to perform the first quantitative analysis of a statistically meaningful sample of OVz stars. Using the FASTWIND stellar atmosphere code they obtained stellar and wind parameters for 38 OVz and 46 OV stars, and found that, in general, the OVz stars appear to be on or very near to the ZAMS, although there are a non-negligible number of cases with more advanced ages of 2-4 Ma. They also investigated the predictions of the FASTWIND code regarding the Vz characteristic, and remarked on the fact that, in addition to effective temperature and wind

strength, other stellar parameters such as gravity and projected rotational velocity must be taken into account for the correct interpretation of the phenomenon from an evolutionary point of view. An interesting conclusion of this exhaustive research concerns the role of metallicity in the O Vz phenomenon. These authors propose that the large number of Vz stars in 30 Doradus, and the fact that some of them are found away from the ZAMS, may be explained by the low metal content of the LMC, which inhibits the development of a wind strong enough to break the Vz characteristic. As a corollary, a lower percentage of O Vz stars away from the ZAMS should be expected in the Galaxy.

In the Galaxy, the Galactic O Star Spectroscopic Survey (GOSSS; Maíz Apellániz et al. 2011) represents the state of the art in spectral classification of massive hot stars. Based on high signal-to-noise (S/N) observations from both hemispheres, it is the largest collection of O-star optical spectra ever assembled. Because of the quality, quantity, and homogeneity of the data, this survey has produced several systemic developments and revisions, some of them unexpected, for the O-type stars. Besides, having improved the definition of the spectral-classification system, GOSSS has revealed numerous objects and categories of special interest, also allowing their statistical study (Walborn et al. 2010; Sota et al. 2011; Walborn et al. 2011; Sota et al. 2014).

The present work constitutes a further example of the potential of GOSSS. Its unprecedented database has confirmed several previously known cases of stars belonging to the O Vz class, as well as led to the discovery of many new examples. Sota et al. (2011, 2014; hereafter S11 and S14, respectively) present spectral classifications for a total of 448 stars, 167 of which belong to the luminosity class V. Among them, 68 objects have been classified as O Vz. More than 150 additional dwarfs have been observed after the publication of the first two papers of the project, the majority of which are included in the third installment (Maíz Apellániz et al. 2016, hereafter MA16). Making use of this huge amount of new data, in this paper we investigate systematically the properties of the O Vz stars in the Galaxy. This empirical analysis is also complemented by a simple theoretical study of the Vz phenomenon (Section 6). With a limited resolving power of $R \sim 2500$, the GOSSS data are not suitable for the determination of the stellar parameters by the use of state-of-the-art stellar atmosphere models¹. Then, following the procedure in the work by SS14, we used synthetic spectra from a grid of FASTWIND models to investigate the effect of several parameters on the occurrence of the Vz spectral peculiarity in a solar metallicity environment.

¹In a forthcoming paper, we will present such a quantitative analysis using high-resolution spectra from two large spectroscopic surveys in the Milky Way: OWN (Barbá et al. 2010) and IACOB (Simón-Díaz et al. 2011a, 2015).

2. Observations

All the observations used in this work come from the Galactic O-Star Spectroscopic Survey (GOSSS). Details about the data and analysis procedures are fully discussed in the three papers of the project (S11, S14, and MA16) and will not be repeated here. We recall only that GOSSS is a long-term systematic survey of all Galactic stars ever classified as O. This project is providing moderate resolution ($R \sim 2500$) spectroscopy in the blue-violet region (approximately 3900-5000 Å), with high signal-to-noise ratio, typically $S/N \sim 200 - 300$. The spectral types are available through the latest version of the Galactic O-Star Catalog (GOSC, Maíz Apellániz et al. 2004). In this paper we include 226 O stars from both hemispheres pertaining to the three published GOSSS installments.

3. Selection criteria for the sample of study

By the beginning of this work, the GOSC contained more than three hundred class-V stars, spanning a spectral-type range from O3 to O9.7. Spectral types for 163 of them had already been published by S11 and S14. We used the original spectral classifications of the latter objects as a starting point for the present study. In Figure 1 the spectral type distributions for them are shown. The top panel shows the distribution for the 68 stars belonging, at that time, to the Vz category, whereas the bottom panel shows that corresponding to the 95 objects classified as “normal” dwarfs, i.e. class V non-z. It must be stressed that these spectral classifications were obtained previously to the introduction of the quantitative criterion defined in this paper². The overall picture was the same as observed for the dwarfs in the 30 Doradus region (see Figure 1 in SS14): the OVz stars showed a marked concentration toward the intermediate spectral type O7, with a complete lack of objects at spectral types later than O8.5, whereas the bulk of the normal dwarfs presented spectral types later than O8.

The observed lack of late-type objects among the OVz stars was not surprising since, strictly speaking, stars with spectral types later than O9 are not relevant to the Vz phenomenon. As was clearly demonstrated by SS14, the Vz spectral characteristic will never be observed at the effective temperatures typical of these objects. Based on models computed for the metallicity of the LMC, these authors showed that below a certain value of T_{eff} , the natural behaviour of the He lines is such that He I $\lambda 4471$ is always stronger in absorption

²In MA16 the Vz classification scheme was adapted to the results presented in this paper; previous spectral classifications were thus revised and modified accordingly.

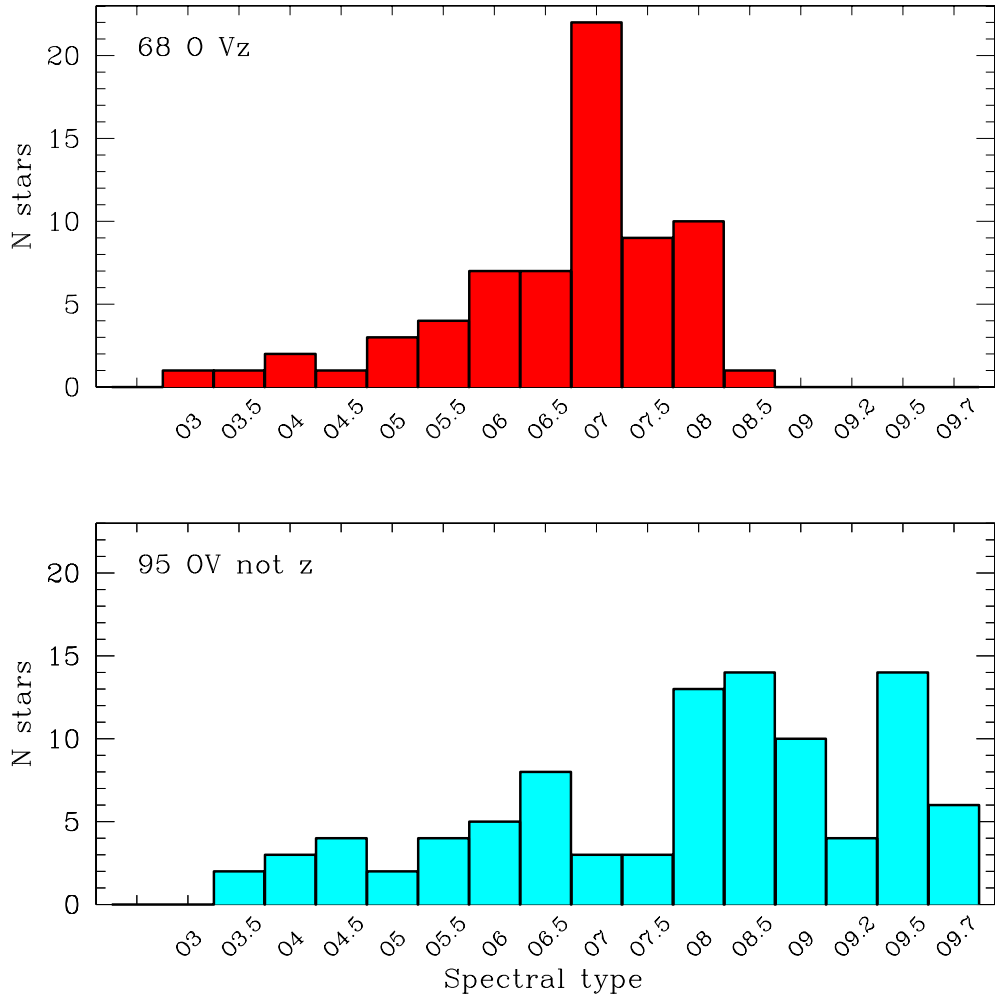


Fig. 1.— Number of stars (N stars) as a function of spectral type for the Galactic O Vz (top) and O V non-z stars (bottom) included in the first two papers of the GOSSS project.

than He II $\lambda 4686$, independently of the wind strength. In Section 6, we will demonstrate that a similar argument is also valid in the Galaxy. In consequence, all the stars with spectral types later than or equal to O9 were not taken into account in the present analysis of the O Vz class. It is interesting to note that, if we restrict the GOSSS published sample to the O3-O8.5 range, the total numbers of objects found at that moment for the Vz and V non-z categories were surprisingly similar (68 and 61, respectively). This means the O Vz objects constituted $\sim 52\%$ of the class V stars in the relevant spectral-type range.

Considering the previous constraint regarding spectral types, our sample of interest decreased to 223 class V stars in the spectral-type range O3-O8.5. These objects have been subdivided into different categories according to the following criteria. As this study involves the measurements of the equivalent widths and central depths of the lines present in the GOSSS spectra, we used the appearance of the spectral lines at the relatively low resolution of GOSSS, along with the available binarity information, in order to separate them into different groups. We will go deeply into the impact of binaries in Section 4.4, but suffice it to say here that they may, for example, produce false O Vz spectra, and hence we had to be extremely careful when probing the binary nature of our sample objects. Additionally to the multiple-epoch GOSSS spectra, information from the literature and/or high resolution surveys was used to identify as many binaries as possible. Then, the categories and numbers that characterize our sample objects are: (1) objects that are single lined in the GOSSS spectra, and for which no evidence of binarity is known (132 stars listed in Table 1); (2) objects that are single lined in the GOSSS spectra, but are known to be spectroscopic binaries (SBs) from high-resolution data (45 binaries, Table 2); (3) objects that are double lined in the GOSSS spectra (explicit SB2), for which the line separation is sufficiently large to allow measurements of central depths and equivalent widths of the individual components by the use of deblending methods (23 binaries providing 32 components with spectral types earlier than O9); and (4) explicit SB2, but whose spectral components are not sufficiently separated to be measured individually (15 binaries). Binaries belonging to groups (3) and (4) are listed in Table 3. A fifth category includes those objects with peculiar spectral characteristics, for example, emission line spectra, magnetic stars, interacting binaries (8 stars). In the following sections the role and significance of each of the former categories will be explained in detail.

4. Spectral classification criteria for the O Vz subclass

4.1. On the problems with the central depth-based classifications

Specifically, the current spectroscopic criterion to assign the luminosity class Vz among O stars is that He II $\lambda 4686$ absorption is *stronger* than any other He line, at every spectral

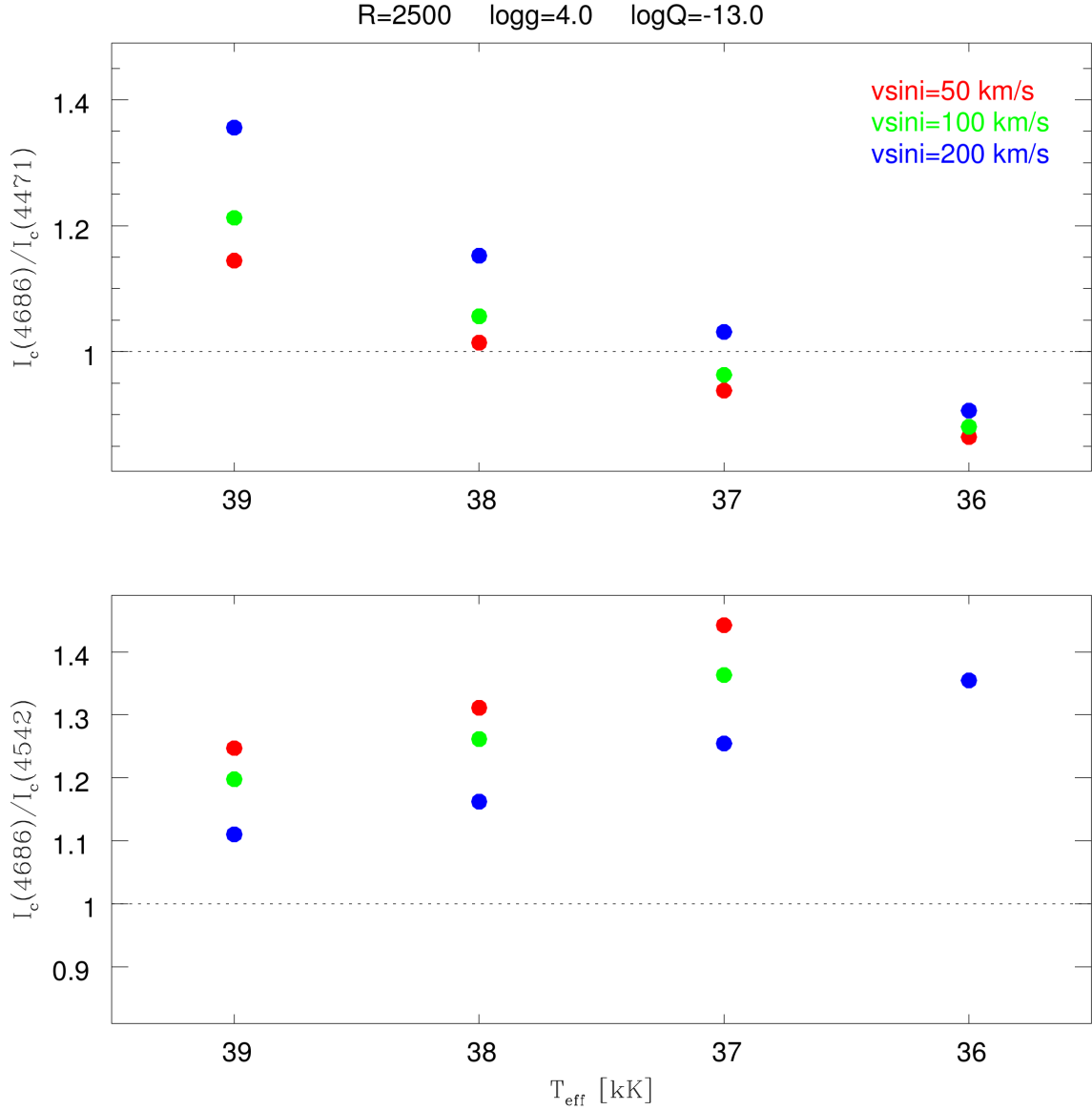


Fig. 2.— Effect of the stellar rotation on the Vz phenomenon defined from the relative depths of the He lines, as shown from FASTWIND model predictions. The intensity I_c is defined as $I_c = 1 - F_c$, where F_c is the flux in the core, and indicates the central depth of the line. A star with effective temperature $T_{\text{eff}} = 37$ kK (corresponding approximately to spectral type O7) may be classified either as Vz or normal dwarf depending on its projected rotational velocity.

type, i. e., it is stronger than He II $\lambda 4542$ at types earlier than or equal to O6.5, stronger than He I $\lambda 4471$ at types later than or equal to O7.5, and stronger than both at type O7 where they are equal by definition.

In the context of the morphological spectral classification scheme, from the advent of the digital data the former criterion is generally applied by comparing the central depths (CDs) of the involved lines. However it is well known that the appearance of the spectral lines may be highly modified by many effects, and that the amount and characteristics of these changes depend on the specific line observed. For example, rotational broadening alters the depths of the He I and He II lines differently, due to the different intrinsic widths of these lines caused by the Stark effect which is linear in He II and quadratic in He I. In particular, the effects of rotation on the spectral types derived morphologically are discussed by Markova et al. (2011). Similar effects may obviously affect the Vz morphological spectral classification. Regarding this point, using FASTWIND models computed for $Z = 0.5 Z_{\odot}$ (corresponding to the metallicity of the LMC), SS14 studied the role of rotational broadening on the Vz phenomenon, finding that, *if we define the Vz characteristic from the relative depths of the He lines*, higher values of $v \sin i$ generally favour the inference of O Vz classifications at relatively low temperatures, with the opposite effect in the high temperature regime.

We explored the former effect using FASTWIND (Santolaya-Rey et al. 1997; Puls et al. 2005) models computed for a metallicity value of $Z = Z_{\odot}$, reasonable for the Galactic stars studied here, and obtained a similar result. A convenient grid of models was chosen among the various included in the IACOB-Grid Based Automatic Tool (IACOB-GBAT; Simón-Díaz et al. 2011b). In Figure 2 the ratio between the CDs of the He II 4686 and He I 4471 absorptions is plotted against effective temperature, for three values of the projected rotational velocity, maintaining the resolution, the surface gravity, and the wind-strength parameter Q fixed³. We note, for example, that the spectrum of a star whose effective temperature is 37 kK (which may reasonably be associated to an O7 spectral type), can be *morphologically* classified either as Vz or “normal” class V, depending on the value of $v \sin i$. Again, in this “low temperature” regime ($T_{\text{eff}} \leq 37$ kK), rapid rotation increases the relevant CD ratio, thus favouring the *CD-based* Vz spectral classification.

On the other hand, the relation between the central intensities and the equivalent widths of the spectral lines depends on various parameters, which leads to the following “paradoxical” result. Let us consider one of the principal horizontal (i.e., spectral-class or temperature) classification criteria for O stars, i.e. the ratio between the intensities of the He I $\lambda 4471$ and

³The wind-strength parameter Q relates the mass-loss rate \dot{M} , the terminal velocity v_{∞} , and the stellar radius R , under the optical-depth invariant $Q = \dot{M}(Rv_{\infty})^{-3/2}$.

He II $\lambda 4542$ lines. By definition, He I $\lambda 4471$ is equal in strength to He II $\lambda 4542$ for type O7.

Using FASTWIND model predictions, we analyzed the variation of the ratios between the CDs and the EWs of the former lines as a function of effective temperature (see Figure 3). We found that, for the considered values of the projected rotational velocity, surface gravity, resolution and wind strength, the CDs of the two lines are equal at $T_{\text{eff}} = T_1 \approx 39$ kK, whereas the equality between their EWs occurs at the much lower temperature of $T_{\text{eff}} = T_2 \approx 36.5$ kK. Current calibrations (Martins, Schaerer & Hillier 2005; Simón Díaz et al. 2014), assign those temperatures to spectral types that differ by at least one subtype. It then seems essential to define a consistent classification criterion.

Walborn & Fitzpatrick (1990) stated that the eye is more sensitive to the EWs of the absorption lines in the photographic spectrograms, but to the CDs in the digital data. Thus, systematic and random differences between the results of the two techniques may be expected. Since EWs cannot be estimated visually in digital data, measurements are indicated as the preferred approach.

4.2. A new “quantitative” classification criterion

Considering the above complications in using only *eye-estimated* CD ratios to define the Vz characteristic, the necessity of taking into account an additional *quantitative* criterion, for example, based on the equivalent widths (EW) of the relevant lines, appears as very reasonable⁴. A first attempt of quantification was done by S14, where the Vz phenomenon was considered as defined by having the ratio:

$$z = \frac{\text{EW}(\text{He II } \lambda 4686)}{\text{Max}[\text{EW}(\text{He I } \lambda 4471), \text{EW}(\text{He II } \lambda 4542)]} \quad (1)$$

greater than ~ 1.0 . This recalibration was obtained by measuring the EWs of the former lines in the main-sequence standard stars. In order to have a deeper insight into the behaviour of the z characteristic, we have now measured the EWs and CDs of the three relevant spectral

⁴We must mention here that, in parallel with the morphological method, an alternative spectral classification method based on the ratios of the EW of certain lines was developed by Conti and collaborators, and subsequently refined by Mathys (e.g. Conti & Alschuler 1971, Conti & Leep 1974, Mathys 1988, 1989). However, this quantitative system is calibrated against the standard MK spectral types, and does not include quantitative criteria for exceptional objects like the O Vz stars, which have been defined exclusively on morphological basis.

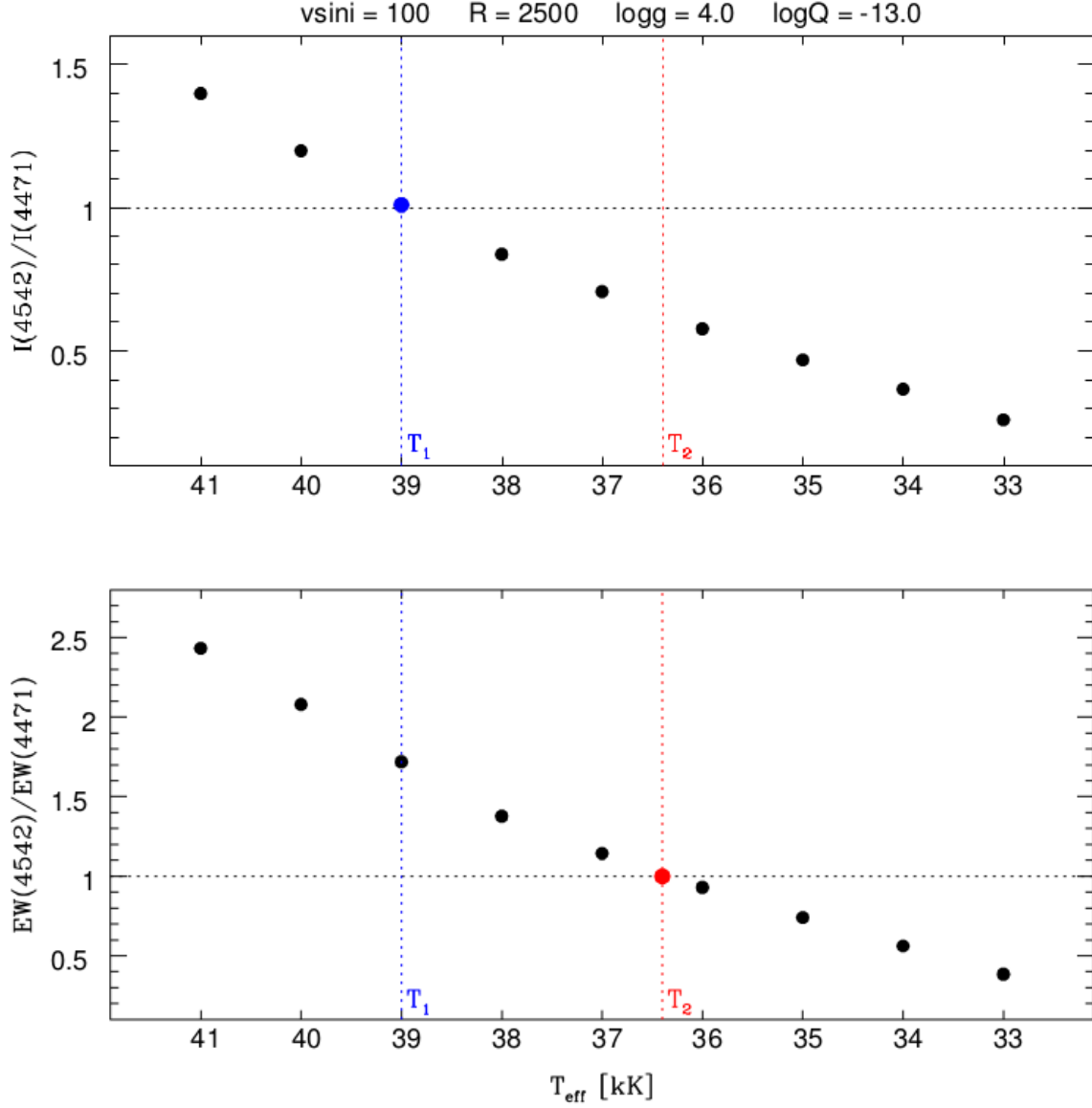


Fig. 3.— Top panel: variation of the ratio between the CDs of the He I $\lambda 4471$ and He II $\lambda 4542$ lines, as a function of T_{eff} , as shown by the FASTWIND model predictions. Bottom panel: the same for the ratio of EWs. Fixed values of the projected rotational velocity, surface gravity, resolution and wind strength have been considered. T_1 and T_2 indicate the effective temperature suitable for the O7 spectral type when considered for its definition the CDs or EWs ratios, respectively.

lines, for a large sample of objects selected among the class V stars in the GOSSS database (see Sections 3 and 4.3 for details about the sample selection).

Because the classification categories are discrete, whereas the phenomena are continuous, spectral classification sometimes requires interpolations or compromises. The Vz classification is not an exception, and the situation may be critical for these stars. Marginal O Vz classifications may be generating confusion in the general picture, and might be, at least in part, the source of the recent controversy regarding the relation between the z characteristic and the youth of the objects. Therefore, in this work we “strengthen” the definition of the Vz phenomenon by increasing to 1.10 the value of the z parameter defined by equation 1, just to avoid those borderline, often unclear, cases. An O dwarf will then be classified as Vz when:

$$z = z_{4542} = \frac{\text{EW}(\text{He II } 4686)}{\text{EW}(\text{He II } 4542)} \geq 1.10 \quad (2)$$

at spectral types earlier or equal to O6.5, and

$$z = z_{4471} = \frac{\text{EW}(\text{He II } 4686)}{\text{EW}(\text{He I } 4471)} \geq 1.10 \quad (3)$$

at types later or equal than O7.5. At the boundary type O7, it must occur than both z_{4542} and z_{4471} are greater or equal than 1.10.

The new critical value for the z parameter was adopted by MA16 in the third installment of the GOSSS project. Besides the reclassification of the dwarfs from S11 and S14 (several of which have changed their “ z status” due to the new more strict requirement of $z \geq 1.10$), this change implied updates on the grid of standard stars used for this task. Moreover it led to the definition, for the first time, of O Vz standard spectra (see Table 2 in MA16). Within the MK scheme of spectral classification, having a complete grid of accurately selected standards is the key for reliable classifications. The quantitative condition $z \geq 1.10$ may also be used to confirm whether or not the z qualifier must be assigned, allowing unclear marginal cases to be objectively resolved.

Spectral classifications and EW measurements for the presumably single stars, single-lined binaries, and double-lined binaries included in our sample of study are compiled in Tables 1, 2 and 3, respectively. For the three tables, column 4 contains the new GOSSS spectral classifications taking into account the above mentioned criteria (reference quoted in column 5). Columns 6, 7 and 8 show the EW measurements for the three He lines involved in the Vz phenomenon, and column 9 includes the z parameter computed from equation 1.

The spectral classifications in the three main GOSSS papers (S11, S14, and MA16) are obtained by a combination of the classical morphological method of visual inspection of the spectra, predominantly determined by the CDs of the lines in the digital data, and the use of MGB (Maíz Apellániz et al. 2012, 2015), an interactive software designed specifically for the project. MGB compares the observed spectrum with a grid of low- $v \sin i$ standards that can be rotationally broadened to simulate the (n), n, nn, and nnn classification suffixes. Therefore, MGB goes beyond the visual CD and line-width estimates, producing results based on the complete profiles of the lines, and compensating the dependence of the CDs on rotation. The results of the two techniques have been intercompared and the final classifications adjusted slightly in some cases. In a future project these classifications will be compared with the measured EW ratios. We have also verified that there is an overall good agreement between the MGB results and the EW determinations of the z characteristic once an appropriate grid of standards is applied. Only for two cases, the double-lined binaries indicated with an asterisk in Table 3, the GOSSS classifications are not in accord with the measured z parameter.

It is interesting to mention that, in the context of the present quantification of the z characteristic, we became aware of several spectra classified as type V with excessively small values of the z parameter, i.e. in the range 0.5–0.7. A number of them were of types O4–O5.5, and inspection from this viewpoint revealed Of morphologies in the GOSSS data well intermediate between most class V spectra and the class III standards, in terms of both the He II $\lambda 4686$ absorption and N III $\lambda 4640$ emission strengths. This finding led to the extension of the range of spectral types for which luminosity class IV is defined. The reader is referred to paper MA16 for details about this recent change.

4.3. Measurements of the spectral lines

As mentioned before, we measured the EWs of the three spectral lines involved in the Vz phenomenon for a large sample of dwarfs selected from the GOSSS database. In Section 3 we explained that, according to the goals of the present work, we excluded stars with spectral types later than O8.5, and divided the 223 remaining dwarfs in the GOSSS database into five different categories. With single-lined features and no evidence of binarity, the 132 objects included in category 1 represent the “simplest” case; all of them have been measured and considered in the analysis related to the Vz class. Their measurements are presented in Table 1. The 23 double-lined binaries in category 3 are also included in the analysis. The measurements of their spectra required the use of deblending methods. As only stars with spectral types earlier than O9 are relevant to the present study, only a few

secondary components, specifically 9 objects, have been measured (see for example MY Cam = BD+56 864 in Table 3).

On the other hand, being unmeasurable, none of the 15 double-lined binaries in group 4 could be considered for the statistics. The peculiar objects in group 5 have not been included either in order to avoid possible sources of noise. This category comprises a total of 8 objects. Finally, group 2 represents a middle situation, as 33 of its 45 binaries have been measured and included in the analysis, whereas 12 have not (see Table 2). We recall that this category comprises single-lined (at GOSSS moderate resolution) spectra of known binary systems. The criterion used to discriminate the useful cases from those that should not be considered for the statistics is the following: the contribution of the secondary to the composite spectrum must be sufficiently small that the measurements obtained from the single spectral features are representative of the primary star. In other words, the presence of the secondary does not alter the resulting spectral z or non- z classification.

To measure the EWs in our spectra, we first attempted to fit (semi-automatically) a Voigt function to the line profiles. This method led to satisfactory fits for the He I $\lambda 4471$ and He II $\lambda 4686$ lines, but not for the He II $\lambda 4542$ line, so the latter had to necessarily be measured manually, i.e., by numerical integration of the line profile between two points selected “by hand” on the continuum. For the sake of uniformity in methodology, we also measured manually the other two He features. It must be recognised that the procedure of rectifying a spectrum is not a trivial task, especially at low resolution, and that local rectification errors, even small ones, can affect significantly the intensities of the spectral features. These uncertainties will impact all the methods of spectral classification, with no exception of course for those based on EW measurements. In particular, the rectification of many O spectra around the He II 4542 line is rather complex, as this feature is intrinsically broader than other He lines, showing also relatively extended wings. Additionally, in most spectra the blue wing appears blended with a set of N III features (4531-4535-4540 Å). Its measurement was thus the most sensitive. In many cases we integrated the red half of the profile and considered the double of that value as the best estimate for the total EW. This effect is particularly important for the extreme cases of N enhanced stars, such as HD 12 993 and HD 110 360, illustrated in Fig. 4. Note that disregarding this blend would enlarge the EW(He II $\lambda 4542$), with a consequent decrease of the z parameter (eq. 1), thus disfavouring the z characteristic.

Because of the reasons explained in the previous paragraph, the errors in the EW measurements cannot be the same for all studied lines. For the usually well-behaved profiles of the He I $\lambda 4471$ and He II $\lambda 4686$ features, the mean absolute error of the EW can be estimated as $\sigma_{4471,4686} \leq 0.02 \text{ \AA}$. Instead, for the more problematic He II $\lambda 4542$ line, absolute errors can

be somewhat larger. Typical values are around 0.03 \AA or smaller but, to be conservative, we adopt a mean value $\sigma_{4542} < 0.05 \text{ \AA}$. The most critical cases regard the EWs of the individual components of double-lined binaries, as deblending methods of measurement generally involve larger errors. For those objects, absolute error values can reach 0.1 \AA . For relative errors of 2% to 7% in the EW measurements, the relative error in the z parameter can be estimated in the range 5 – 10%.

4.4. The effect of binaries

The high degree of multiplicity is a striking characteristic of massive stars (Mason et al. 2009, Barbá et al. 2010, Sota et al. 2014, Sana et al. 2013, 2014), and also one of the most troublesome points when studying these objects. Unknown binaries can easily give rise to wrong conclusions. With respect to the Vz classification, the most critical effect is that they may produce false O Vz spectra. We have identified a few stars from the GOSSS database that appear as nice intermediate O Vz but have subsequently been resolved into a pair composed of an early and a late component, by means of either other GOSSS spectra or additional high-resolution observations. In such an O binary, the early component dominates He II $\lambda 4542$, and the late component dominates He I $\lambda 4471$, but both contribute comparably to the enhanced He II $\lambda 4686$. The case of the multiple system HD 64315 illustrates this situation (see Figure 5). This star is composed of at least two (probably more) components (Mason et al. 2009, Tokovinin et al. 2010, Lorenzo et al. 2010), but, if its spectral lines were measured during the orbital conjunction, the obtained z parameter would reach 1.14, and hence the star would be classified as Vz. Given the high binary frequency among O stars, one may expect not a few HD 64315-like cases, in which a hidden multiplicity is the actual origin for the observed Vz spectrum.

We have been extremely careful when probing the binary nature of our sample objects. Within the GOSSS database, spectra obtained in more than one epoch are available for many stars, which allowed the identification of some spectroscopic binaries. However, we still expected a likely important fraction of unresolved binaries among our sample, due to the limited resolution of the data. Therefore, in order to identify as many binaries as possible, we carefully searched for information from the literature, and also took into account results from high-resolution surveys coordinated with GOSSS like OWN and IACOB. These high-resolution monitoring programs appear in fact as an essential complement for a correct interpretation of the observed statistics.

The misleading origin for some O Vz spectra provided by unknown binaries may obviously be confusing the statistical interpretations. But even if they do not produce false

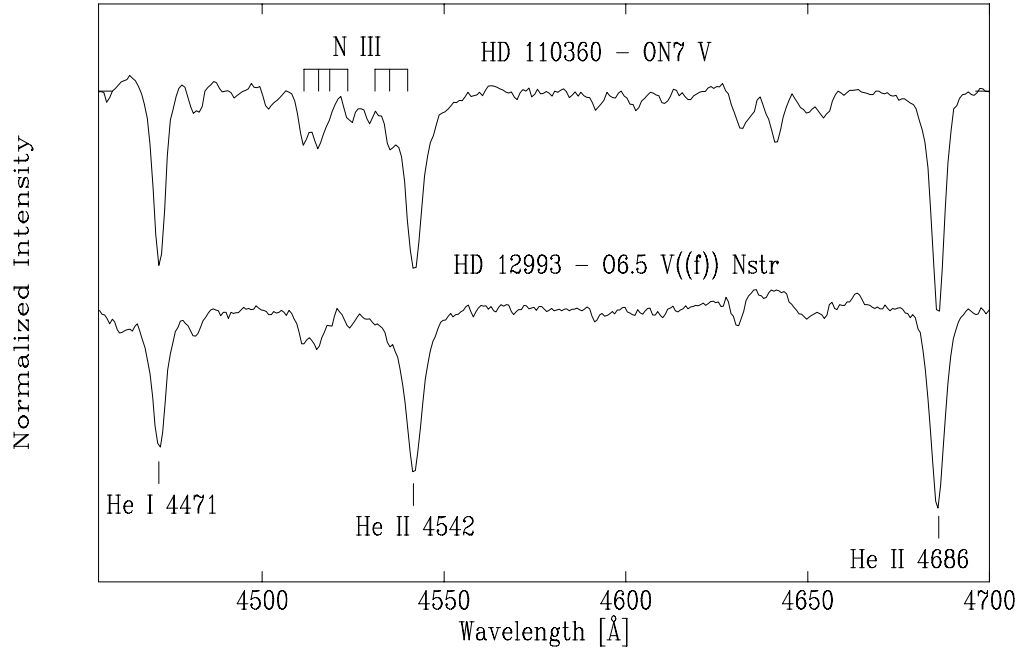


Fig. 4.— Examples of He II $\lambda 4542$ profiles whose EW measurement requires special care, due to the blend with unusually strong N III lines at 4531-4535-4540 Å.

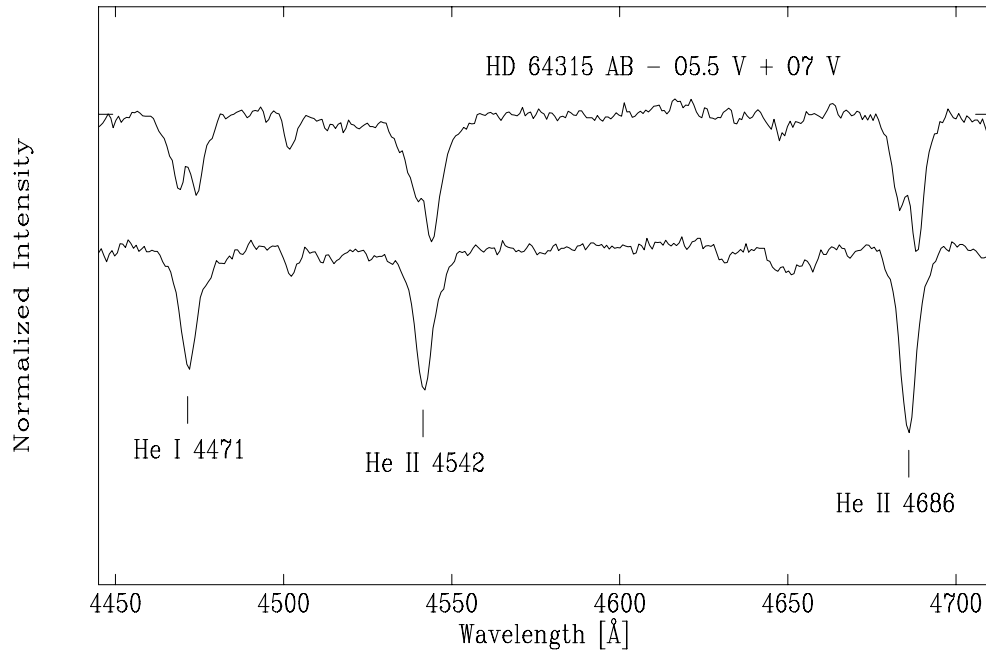


Fig. 5.— Two spectra of the multiple system HD 64315 illustrating how binaries may produce false O Vz spectra. If measured during the orbital conjunction, the z parameter of the composite spectrum is $z=1.14$.

Vz objects, unresolved binaries may be “blurring” the statistical numbers, by leading us to count one object when actually there are two. Among our sample of 223 O dwarfs, we have identified 45 objects whose spectra are single-lined at GOSSS resolution (group 2), although they are known to be binaries from higher resolution spectroscopic or imaging data. A recent result by Sana et al. (2014) claims a fraction of 100% for the luminosity class V stars that have a bound companion within 30 mas. So the key question is how many of the 132 stars *assumed* to be single in this work are actually single. Further investigation is needed but meanwhile we must deal with this uncertainty.

5. The GOSSS O V and O Vz populations

Having addressed the methods applied and the problems arising in their application, we now analyze the resulting populations of O V and O Vz stars in the GOSC.

We recall that our 223 O dwarfs were divided into different categories according to their binary status and the appearance of their spectra, and that not all of them could be measured and included in the present analysis (see Sections 3 and 4.3). After “cleaning” the sample, our final group of study, i.e. those stars for which a confident value of the z parameter can be derived, decreased to 132 presumably single stars, plus 56 binaries or higher order multiple systems, 23 of which are double-lined at the moderate GOSSS resolution allowing individual measurements for 9 additional secondary components. A total of 197 individual stars with spectral types earlier than O8.5 were measured allowing us to apply both the classical morphological and the new quantitative criteria for their spectral classification. We restrict our sample to this set for the statistical considerations on the O V and O Vz populations.

In Figure 6 the z parameter computed from the EWs of the 197 measured stars (along with additional information described afterwards) is plotted as a function of spectral type. Note the large range of z values observed for most of the spectral types. The O dwarfs originally classified as Vz by S11 and S14 have been marked with red squares. We recall the former spectral classifications were obtained regardless of the quantitative criterion proposed in the present work. In the same figure, we have marked with a solid line the condition $z \geq 1.10$ which represents the threshold to assign the z qualifier proposed here. Only those O dwarfs whose z parameters fall above this line are now classified as Vz. Slightly bigger black circles denote these cases. The representative point on the lower left corner of the figure shows the typical uncertainty in the z parameter. Note that, for objects with z close to the threshold, measurement errors might change their “ z status”. Some examples of spectrograms, in particular for the most extreme cases, are shown in Fig. 7.

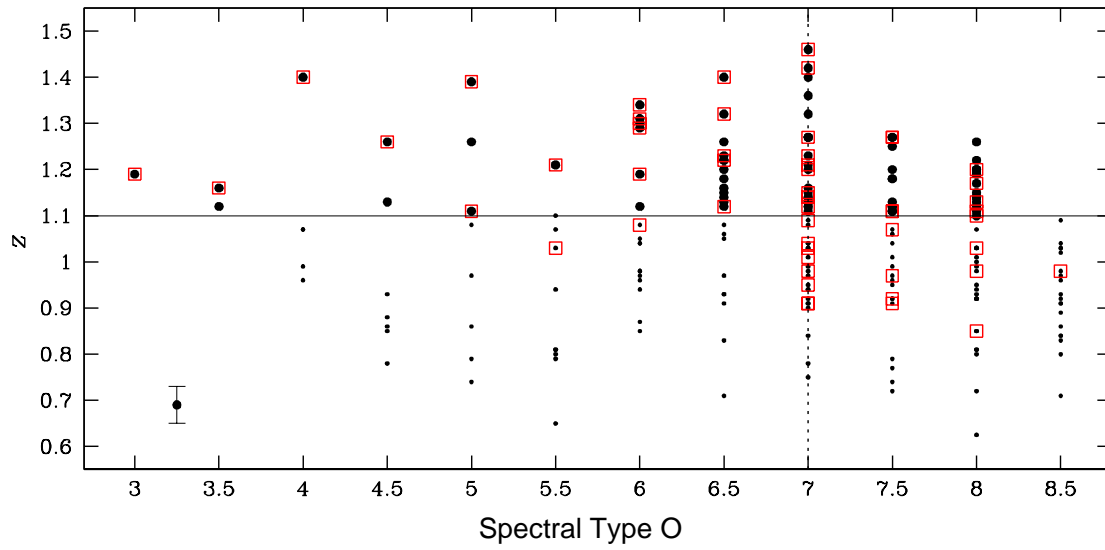


Fig. 6.— The z parameter computed from the EWs measured in the GOSSS class-V spectra, as a function of spectral type. The red squares surround O Vz classified previously to the introduction of the quantitative criterion proposed in this paper. The solid line at $z = 1.10$ indicates the current threshold to assign the z qualifier. Only the points above this line correspond to the newly classified O Vz. The representative point with error bars on the lower left corner of the figure illustrates the typical uncertainty in the z parameter.

The spectral type distribution observed for the newly classified O Vz stars is presented in the top panel of Figure 8. For comparison, an analogous distribution for the “normal” class V objects spanning the same spectral type range is included in the middle panel of the same figure. The bottom panel shows relative differences between the two populations for each spectral type.

With the addition of the new quantitative classification criterion, the O Vz population decreased to 78 members, and thus they represent $\sim 40\%$ of the class V stars in the relevant spectral-type range, a significantly lower fraction, compared with the 52% corresponding to morphology-only-based classifications. More importantly, the distribution for the “normal”, i.e. non-z, dwarfs does not show that deficiency of objects with intermediate spectral types O7-O7.5 observed in the histograms in Figure 1. Among the Vz stars however there is still a predominance of intermediate-type objects. Specifically, 61 O Vz objects, $\sim 78\%$ of the whole sample, show spectral types between O6.5 and O8. As evident from the bottom panel of Figure 8, the populations of O Vz and O V non-z stars are comparable in number at the former subtypes.

We would like to compare the newly obtained spectral type distribution with that for the O V stars in 30 Doradus (Fig. 1 of SS14). However the two Vz samples were selected following different criteria, as the restrictive quantitative condition $z \geq 1.10$ was incorporated in this paper for the first time. A detailed comparison will make sense only after the classification methodology is standardized. In any case, both distributions share overall characteristics such as, for example, the mentioned predominance of intermediate types among the Vz stars. Using FASTWIND model predictions, SS14 show that part of the properties of the O Vz and O V stars in 30 Doradus can be explained by a natural combination of stellar parameters. In Sec. 6 we carry out a similar procedure to investigate the occurrence of the Vz phenomenon (defined not from the CDs but from EWs of the He lines) in a solar-metallicity environment. We shall show that the distributions in Fig. 8 are in good agreement with what it is predicted by the models.

6. FASTWIND model results

In a way very similar to that followed by SS14, we use synthetic spectra computed with the FASTWIND stellar atmosphere code to investigate how the variation of the most relevant parameters, namely, wind strength (Q) and effective temperature (T_{eff}), impact in the occurrence of the Vz peculiarity. The differences with the former analysis are twofold: first, we use a grid of models computed for the solar metallicity $Z = Z_{\odot}$, which is an appropriate mean value for the GOSSS stars; and second, we consider the quantitative

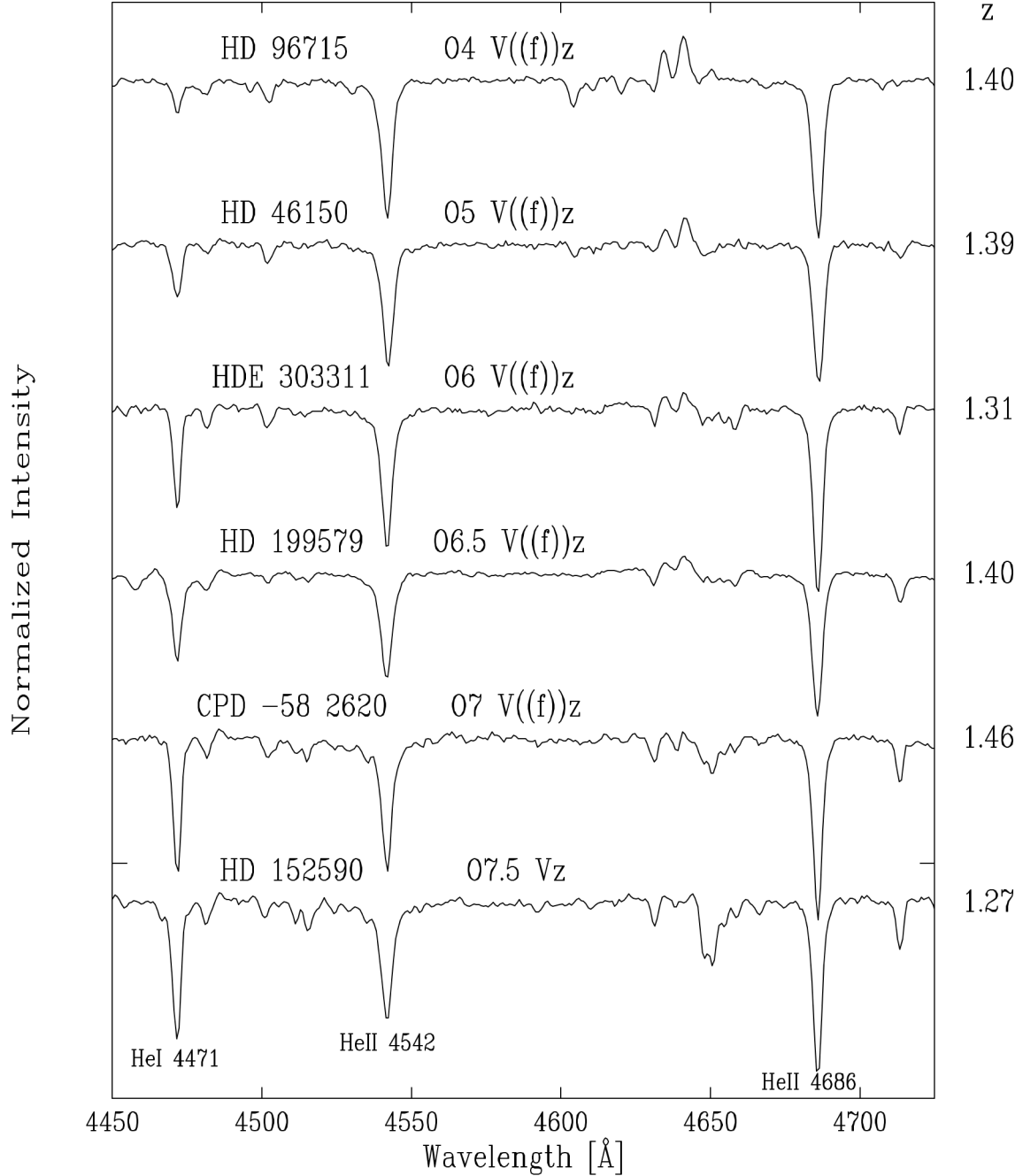


Fig. 7.— Examples of GOSSS spectra for some of the most extreme cases belonging to the O Vz class. The rectified spectrograms are separated by 0.2 continuum units. The corresponding z parameter is indicated to the right of each spectrum.

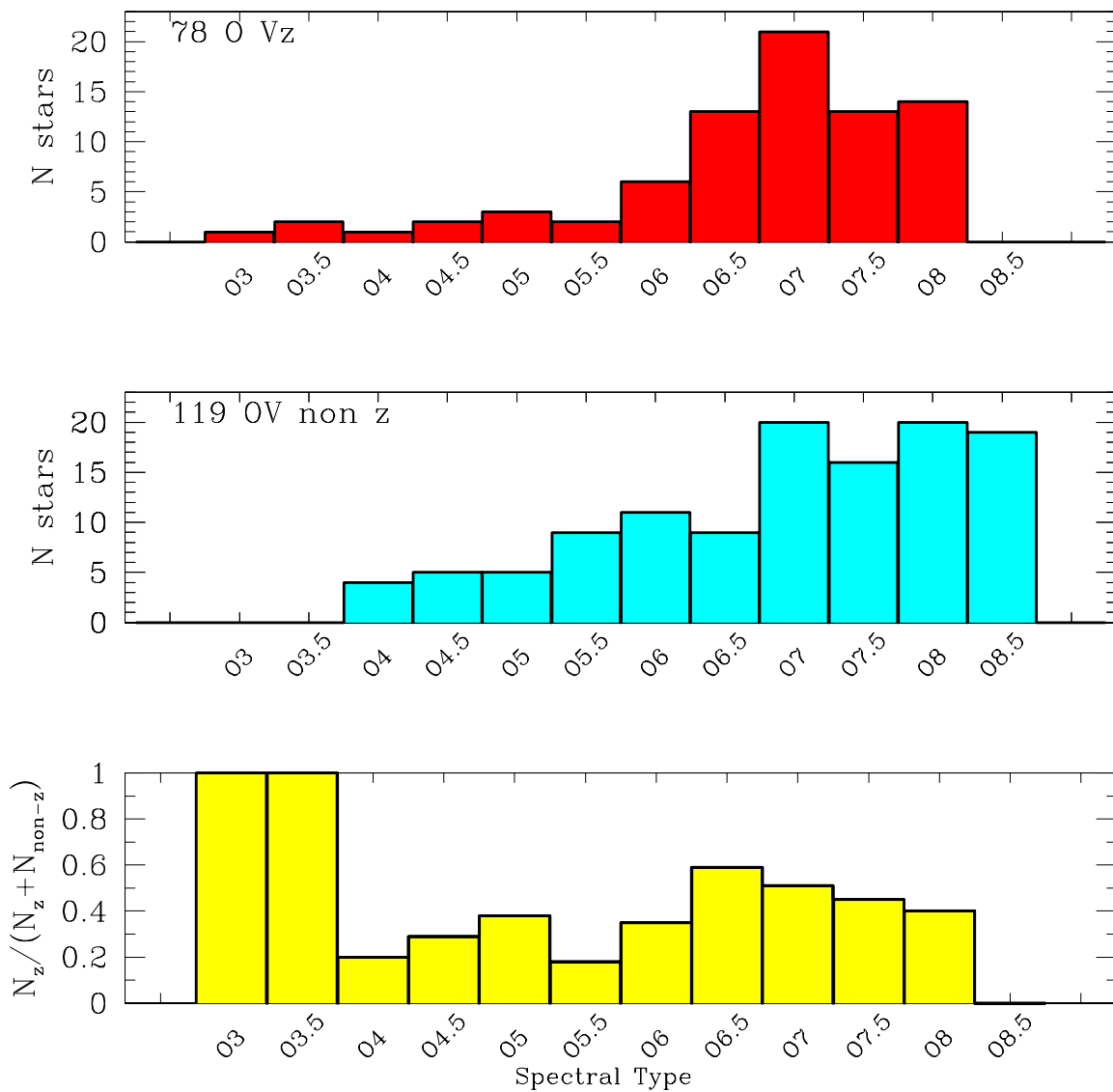


Fig. 8.— Number of stars (N stars) as a function of spectral type for the Galactic O Vz (top panel) and O V non-z stars (middle panel) included in our GOSSS sample of study. The bottom panel shows the number of Vz objects relative to the total number of class-V stars at each spectral type.

criterion based on the EWs of the He I $\lambda 4471$, He II $\lambda 4542$, and He II $\lambda 4686$ lines (see Sec. 4.1) for the definition of the Vz characteristic. The main conclusions from the present analysis are qualitatively the same found by SS14, who were the first to point out the importance of taking into account additional parameters to interpret correctly the Vz phenomenon. However numerical results are somewhat different, most probably due to the distinct values of the metallicity considered in each case.

As discussed in Sec. 4.2, an O7 dwarf will be classified as Vz when both z_{4542} and z_{4471} are greater or equal than 1.10. The effective temperature for this boundary type is represented by T_2 in Figure 3. For the values of projected rotational velocity, surface gravity, resolution, and wind strength indicated at the top of that figure, T_2 is between 36 and 37 kK. Although it depends on the specific values considered for the former parameters, such a value is a reasonable estimate for the limit between the use of z_{4542} and z_{4471} .

We first study how z_{4542} and z_{4471} behave with the variation of the wind strength Q -parameter. Fig. 9 shows these parameters as a function of $\log Q$ for a set of different values of the T_{eff} , ranging from 35 to 38 kK for z_{4471} (top panel), and from 37 to 41 kK for z_{4542} (bottom panel). Resolution, surface gravity, and projected rotational velocity are fixed for simplicity. In both panels, the dash-dot line at $z = 1.10$ marks the value upon which the star is classified as Vz.

The first conclusion that arises from the top panel of Fig. 9 is that O spectra with effective temperatures below a certain value (which is close to 35 kK) will never be classified as Vz. No matter how weak the stellar wind is, the z parameter for the latest-type stars never exceeds the adopted threshold. This conclusively justifies the decision to exclude all the dwarfs with spectral types later than O8.5 from the very beginning of the study (Sec. 3).

Fig. 9 also shows that at higher temperatures the stars may show the Vz characteristic until the Q parameter takes a certain value denoted as Q_{lim} . This limit value of Q would represent the strength of the wind required to sufficiently fill in the He II $\lambda 4686$ absorption, so the condition $z > 1.10$ is broken and, as already shown by SS14, is highly dependent on T_{eff} . In a solar-metallicity environment, Q_{lim} takes its largest value at 37 kK, considering either z_{4542} or z_{4471} (in the upper panel, the curve for 38 kK is included for reference, but this temperature is very likely out of the z_{4471} relevant range). Therefore, the main-sequence stars whose T_{eff} are close to 37 kK are those that need the strongest stellar winds to no longer show the Vz peculiarity in their spectra. This may explain the predominance of intermediate spectral types in the histogram of Fig. 8.

The bottom panel of Fig. 9 shows that for very early objects with T_{eff} above ≈ 39 kK, the Vz characteristic may vanish much before the development of a strong wind; in other

words, these stars could be classified as non-z even if they have stellar winds with a strength comparable to other O Vz at later types. This naturally explains the observed drop in the number of O Vz stars for spectral types earlier than O6.

In the present model configuration, the approximate values of $\log Q_{\text{lim}}$ are: -12.85 for $T_{\text{eff}} \approx 37$ kK (or -13.1 , if considered z_{4542}), -13.20 for $T_{\text{eff}} \approx 36$ kK, and lower than -13.35 for T_{eff} of the order and above 38 kK. We recall that, in this model, the resolution, surface gravity, and projected rotational velocity are fixed for didactic purposes ($R = 2500$, $\log g = 4.0$, and $v \sin i = 100$). Although the overall behaviour of the z parameter is similar, the limit values of Q can logically vary when alternative configurations are considered, i.e. for different values of R , $\log g$, and $v \sin i$, which is a fortunate fact as the existence of Vz stars with $T_{\text{eff}} > 39$ kK would be otherwise very difficult to explain. Anyway, Q_{lim} for $T_{\text{eff}} \approx 37$ kK always appears to be significantly larger than those computed for other effective temperatures. As a conclusion we may say that, in a solar metallicity environment, the O-type stars with effective temperatures close to that value are by far the most “favoured by nature” to show the Vz characteristic in their spectra. This fact is in complete agreement with the observed statistics.

We would like to emphasise that the goal of the very simple theoretical analysis performed here is to contribute to understanding the observations, in particular, the behaviour of the measured EWs, as well as the spectral-type distribution observed for the Galactic O Vz and O V stars. Thus, we show that FASTWIND model predictions can nicely account for some of the observed characteristics. These results neither contradict nor confirm the hypothesis of the extreme youth of the Vz stars, but only evidence, as already done by SS14, the importance of considering several stellar parameters related to different physical processes when interpreting the Vz phenomenon.

7. Locations of the Vz stars

When investigating a peculiar or new class of stars, it is important to also consider their environments and companions, which may provide clues to their nature. The initial hypothesis regarding the Vz class was that it might be younger than the typical class V, based upon the “inverse Of” interpretation of the phenomenon as explained in the Introduction. Thus, we discuss the locations of the Vz stars in this section, with special attention to the most extreme members of the class. In an attempt to quantify the definition of an “extreme” Vz star, we will consider the condition $z \geq 1.20$. Although somewhat arbitrary, this limit is useful since ensures the membership to the Vz class, even in the cases where measurement errors are large and, at the same time, focus the discussion on the most particular objects,

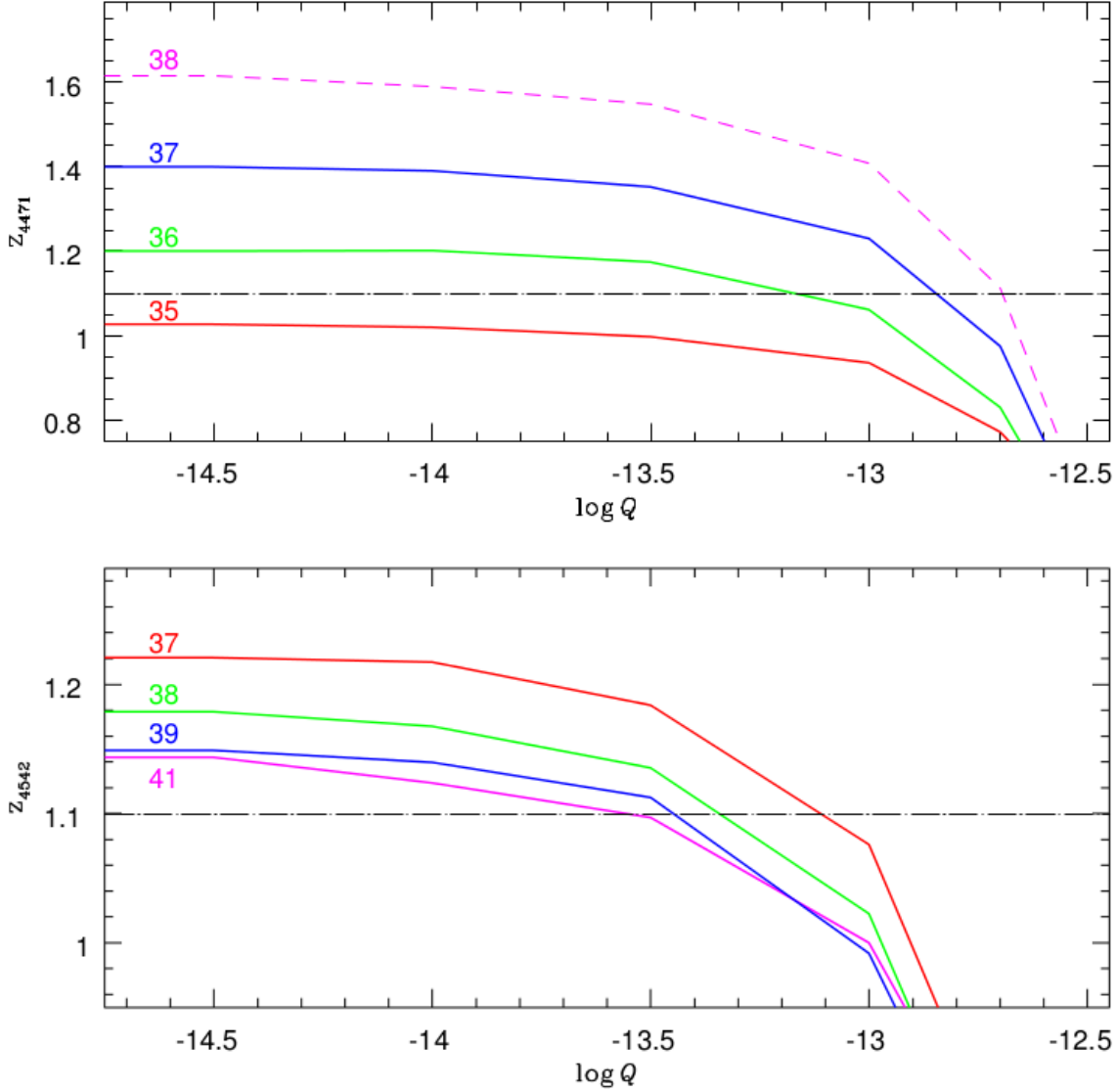


Fig. 9.— FASTWIND predictions of the behaviour of the EW ratios that define the z spectral characteristic, with the variation of the wind-strength parameter Q . Fixed values of the resolution ($R = 2500$), surface gravity ($\log g = 4.0$ dex), and projected rotational velocity ($v \sin i = 100 \text{ km s}^{-1}$) have been considered. The labels next to each color curve indicate the corresponding effective temperature expressed in kK. In the upper panel, the dashed line for 38 kK indicates that this temperature is likely out of the z_{4471} relevant range.

such as for example those shown in Figure 7, for which the depth of the He II $\lambda 4686$ absorption relative to the other He lines is really striking.

Table 4 lists the clusters and H II regions containing Vz objects from our current sample of 197 luminosity-class V, i.e dwarfs, stars. The number of z dwarfs within each cluster is quoted in the third column of the table. The number of non-z dwarfs is also provided for comparison in the last column. Of course, these numbers are lower limits not only because of observational incompleteness, but also due to the selection criteria for the measurable sample (Sec. 3). Column 4 details the names of the z dwarfs in each cluster. The 39 “extreme” members, as defined previously, are marked in bold. As a comparison and control, Table 5 provides an analogous listing for the clusters that contain normal, i.e. non-z, dwarfs, but do not include Vz objects.

Table 4 contains 52 Vz stars in 15 clusters and/or H II regions that contain two or more Vz objects, all of which have ages less than about 3 Ma insofar as is known; at greater cluster ages, H II regions are generally absent (Walborn 2010). The same Table also includes 23 single (to date) Vz stars in 23 young clusters and/or H II regions, for a grand total of 75 found in such environments. Only three Vz objects (HD 19265, HD 44811, and HD 97966), cannot be directly associated to a very young cluster. The especially outstanding entries in Table 4 are the Carina Nebula with a total of 19 Vz members, half of which are extreme cases, and the extended Cygnus region with 12, distributed among various subregions in both cases. The Vz content of the IC 1795/1805/1848 complex, and other clusters such as NGC 6611 and NGC 1893, is also notable. These are all very young objects, providing support for that interpretation of the Vz class.

Besides the large absolute number of Vz stars in Carina and Cygnus, which might be expected since those are the two best-represented regions in GOSSS, the proportion of Vz to normal class V objects ($\sim 60\%$) is evident. Within the Carina Nebula, the difference between Trumpler 14 and Trumpler 16 is particularly curious. While the former shows a majority of z objects, in the latter there is a predominance of non-z dwarfs. Some authors have suggested an extremely young age around 0.5 Ma for Trumpler 14 (e.g. Penny et al. 1993; Rochau et al. 2011). On the other hand, although also very young, Trumpler 16 appears somewhat older (e.g. Wolk et al. 2011) with evolved supergiants like the remarkable Luminous Blue Variable η Car.

Among the clusters with no Vz objects (Table 5), we emphasize IC 2944, which contains at least 3 normal dwarfs (5, if the binaries HD 101131 AB and HD 101436 are also taken into account), and shows a tenuous H II region. McSwain & Gies (2005) evaluated the age of IC 2944 to be 6.6 Ma. Other salient cases are Havlen-Moffat 1, an evolved cluster containing Wolf-Rayet stars (Havlen & Moffat 1977), and also IC 1590 and NGC 6604,

whose average ages are found to be larger than 6.0 Ma (Kharchenko et al. 2013). All the clusters from Table 5 are on average older than those containing a conspicuous population of O Vz objects, as suggested by the different morphologies observed in the mid-infrared images from the *Wide-field Infrared Survey Explorer* (*WISE*) (Figure 10). The change in the morphology of a massive star forming region with the evolutionary stage of the underlying massive stellar content is nicely presented by Koenig et al. (2012). Using the *WISE* images in the W3 channel ($12\ \mu\text{m}$), these authors show the correlation between the age of the main exciting stellar cluster and the structure of the diffuse emission nebulosity produced by excited polycyclic aromatic hydrocarbon molecules (PAH) and small dust grains. Younger massive stellar clusters lack a cleared out cavity around the powering O stars. Within a timescale of 3 – 5 Ma, the H II regions are cleared out and the observed PAH and dust emission is mostly concentrated in peripheric ring structures with protuberances or pillars where a new, triggered generation of stars is forming. This evolutive scenario of massive star formation was previously depicted by Walborn & Parker (1992) (see also Walborn et al. 1999) and named "two-stage starbursts" scenario.

Finally, in Figure 11 we present the spatial distribution of the Galactic z (red circles) and non-z (cyan circles) O dwarfs, overplotted on the H α all-sky map produced by Finkbeiner (2004). The Vz objects, especially the most extreme, seem to show a higher concentration toward the most active star forming regions. Of course, normal dwarfs are also found within these regions but, as a class, the latter appear more disseminated within and out of the Galactic disk. As a conclusion we can say that, while further astrophysical investigation is needed, the extreme Vz objects may reasonably be hypothesized to represent the youngest, post-embedded massive stars.

8. Summary and outlook

Comprising the largest collection of O-star optical spectra ever assembled, The Galactic O Star Spectroscopic Survey (GOSSS) provides a unique opportunity to investigate in detail and systematically this important class of objects. The O stars belonging to the Vz luminosity subclass have been suggested to be among the youngest optically observable massive objects, and thus their study appears as key to the understanding of the early evolution of massive stars.

This work provided a new insight into the Vz spectral classification criteria. The convenience of incorporating a quantitative criterion based on the equivalent widths (EWs) of the He I $\lambda 4471$, He II $\lambda 4542$, and He II $\lambda 4686$ spectral lines was shown. The EWs for a large sample of stars in the Galactic O Star Catalogue (GOSC) were measured, allowing the re-

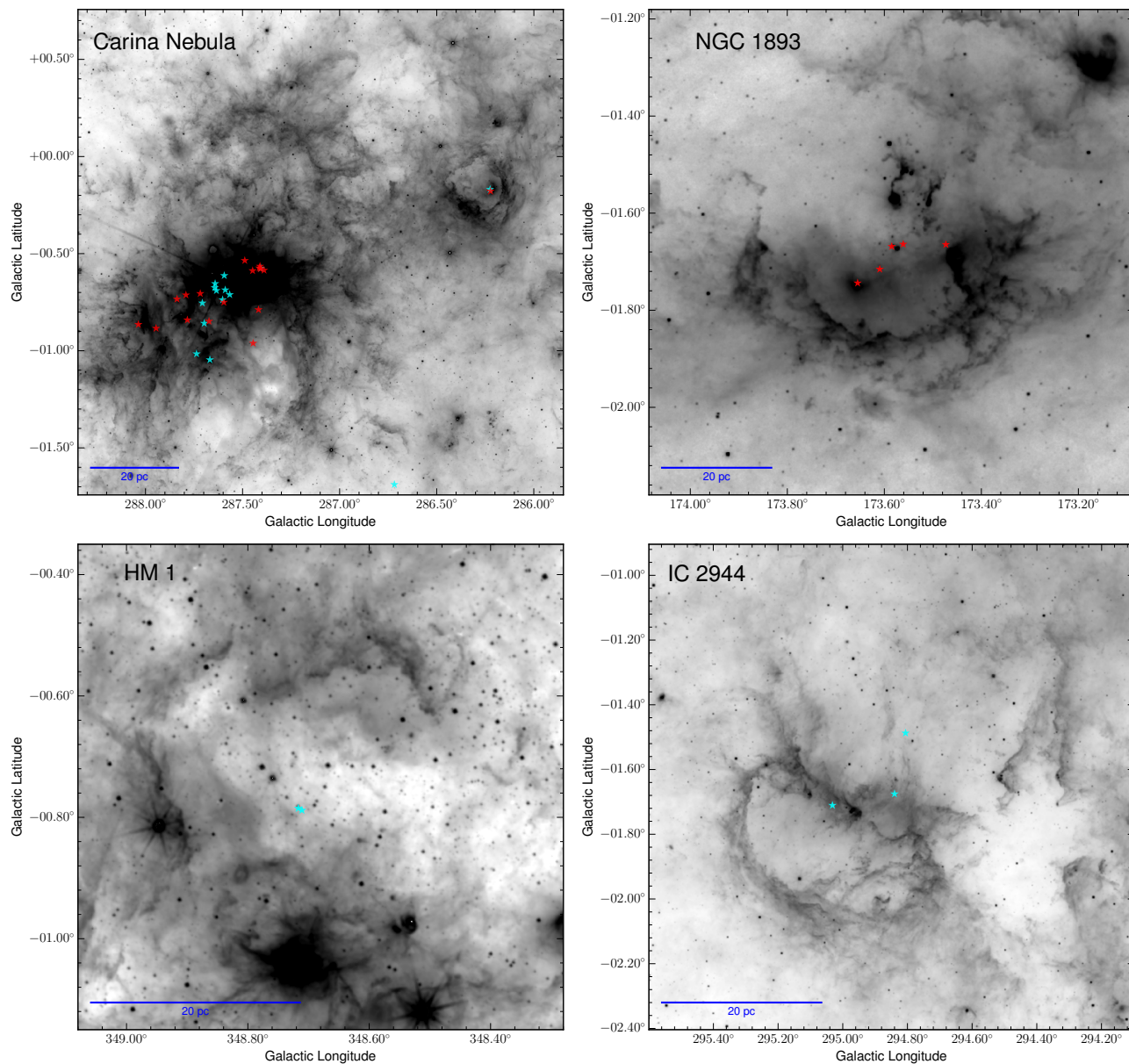


Fig. 10.— Spatial distribution of Galactic O Vz (red stars) and O V (cyan stars) objects in selected H II regions. The background images correspond to the $12\ \mu\text{m}$ W3 channel of the *Wide Infrared Space Explorer* (*WISE*) represented in Galactic coordinates. The scale bar represents a length of 20 pc according to the distance proposed for each region. Top: Carina region (left) and NGC 1893 (right). Bottom: Havlen-Moffat 1 (left) and IC 2944 (right).

calibration of the Vz phenomenon. As a result, the threshold of the “ z parameter”, defined as $z = \text{EW}(\text{He II } \lambda 4686) / \text{Max}[\text{EW}(\text{He I } \lambda 4471), \text{EW}(\text{He II } \lambda 4542)]$, upon which a spectrum is classified as Vz, was increased to 1.10. This change aims to avoid marginal cases, whose actual membership to the Vz class is unclear and may be therefore contributing to the recent controversy arising regarding the relation between the Vz classification and the small age of the objects. The new critical value for the z parameter proposed in this work was adopted in the third installment of the GOSSS project. This led to a complete revision of the spectral types in GOSC and, more importantly, to the definition for the first time, of O Vz standard stars.

The population of O V and O Vz stars resulting from the new classification criteria were comparatively analyzed. With 78 members, the O Vz objects represent $\sim 40\%$ of the dwarfs in the relevant spectral range of O3-O8.5. However their distribution as a function of spectral type is not uniform but shows a marked concentration toward intermediate types. Based on a very simple theoretical analysis performed using synthetic spectra from a grid of FASTWIND models computed for a solar-metallicity value, we showed that the former, as well as other observed characteristics in the spectral-type distribution of the O Vz stars, are in perfect agreement with what is predicted by the models. This study confirmed the result from SS14 about the complexity, previously unrecognized, of the Vz phenomenon and the necessity of taking into account many processes for its correct interpretation.

The locations, environment, and companions of the O Vz stars were analyzed, with special attention to the most extreme members. Almost all of the O Vz objects are associated with very young clusters, all of which have ages less than 3 Ma insofar as is known. On the other hand, clusters with no Vz objects are clearly older, as evidenced by the morphologies observed in the mid-infrared WISE images, and the presence of more evolved stars. These facts add considerable support for the interpretation of the Vz characteristic as a signature of youth, although further astrophysical investigation is needed.

The results presented here represent the first steps toward our goal of understanding the physical significance of the O Vz stars. We have defined a robust sample of O Vz stars, many of them presumably single, suitable to perform quantitative spectroscopic analyses in high-resolution which will allow us to derive their stellar and wind parameters. Such a study, aimed to be presented in a forthcoming paper, will certainly establish the actual evolutionary status of these interesting objects.

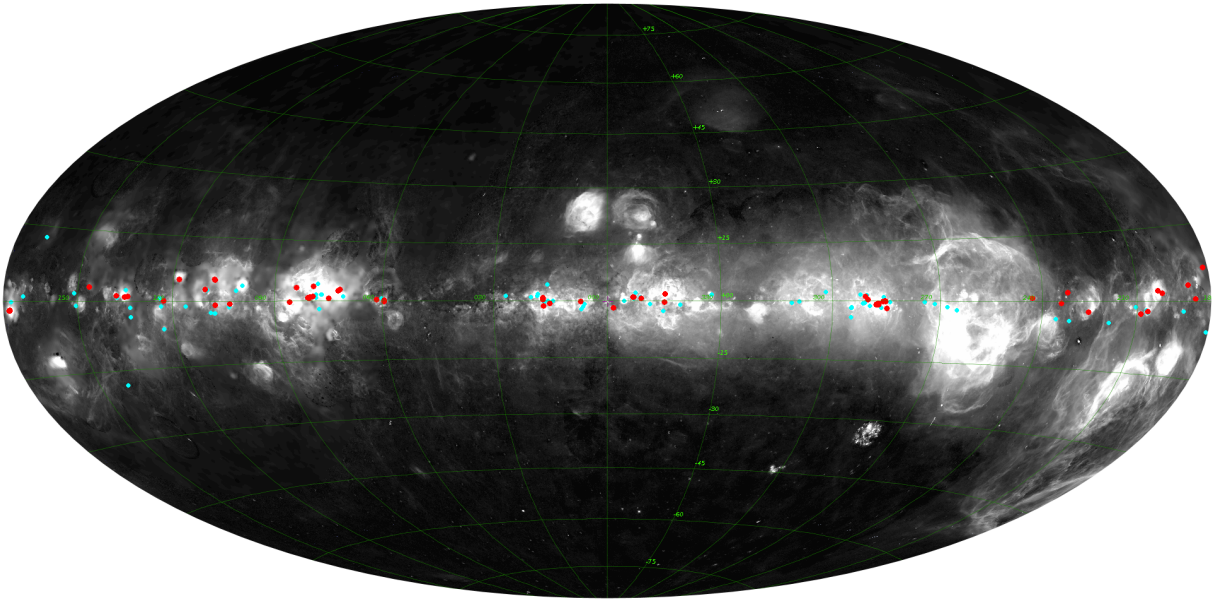


Fig. 11.— Spatial distribution of Galactic O Vz (red circles) and O V (cyan circles) stars included in our sample. The background image is the H α map in Aitoff projection produced by Finkbeiner (2004) and represented in Galactic coordinates.

Table 1. O V stars in GOSSS with no evidence of binarity

Object	R.A. hh:mm:ss.ss	Decl. dd:mm:ss	Sp. Type	Ref.	EW(He I 4471) [Å]	EW(He II 4542) [Å]	EW(He II 4686) [Å]	<i>z</i>
BD +66 1675	00:02:10.29	+67:24:32.2	O7.5 Vz	MA16	0.70	0.68	0.88	1.25
Tyc 4026-00424-1	00:02:19.03	+67:25:38.5	O7 V((f))z	MA16	0.55	0.66	0.84	1.27
ALS 6351	00:48:12.55	+62:59:24.8	O7 Vz	MA16	0.71	0.90	1.04	1.16
HD 5005A	00:52:49.21	+56:37:39.5	O4 V((fc))	S11a	0.19	0.76	0.81	1.07
HD 5005C	00:52:49.55	+56:37:36.8	O8.5 V(n)	S11a	0.85	0.81	0.76	0.89
BD +60 134	00:56:14.22	+61:45:36.9	O5.5 V(n)((f))	MA16	0.50	0.91	1.00	1.10
HD 5689	00:59:47.59	+63:36:28.3	O7 Vn ((f))	MA16	0.70	0.92	0.71	0.78
HD 12993	02:09:02.47	+57:55:55.9	O6.5 V((f)) Nstr	S14	0.70	0.95	1.00	1.05
BD +61 411 A	02:26:34.39	+62:00:42.4	O6.5 V((f))z	MA16	0.46	0.73	0.89	1.22
BD +60 501	02:32:36.27	+61:28:25.6	O7 V(n)((f))z	S11a	0.57	0.75	0.91	1.21
HD 15629	02:33:20.59	+61:31:18.2	O4.5 V((fc))	S11a	0.20	0.66	0.52	0.78
BD +60 513	02:34:02.53	+61:23:10.9	O7 Vn	MA16	0.61	0.82	0.75	0.91
BD +62 424	02:36:18.22	+62:56:53.4	O6.5 V(n)((f))	S11a	0.45	0.80	0.73	0.91
HD 17505B	02:51:08.26	+60:25:03.8	O8 V	S11a	0.70	0.54	0.69	0.99
BD +60 586 A	02:54:10.67	+60:39:03.6	O7 Vz	S11a	0.68	0.67	0.83	1.23
ALS 7833	03:59:07.49	+57:14:11.7	O8 Vz	MA16	0.72	0.70	0.87	1.20
BD +50 886	04:03:20.74	+51:18:52.5	O4 V((fc))	MA16	0.12	0.74	0.79	1.07
BD +52 805	04:18:35.64	+52:51:54.3	O8 V(n)	MA16	0.80	0.77	0.86	1.07
ALS 8294	05:22:39.69	+33:22:18.2	O7 V(n)z	MA16	0.83	0.81	0.93	1.12
HDE 242926	05:22:40.10	+33:19:09.4	O7 Vz	S11	0.61	0.77	0.88	1.14
BD +33 1025 A	05:22:44.00	+33:26:26.6	O7.5 V(n)z	S14	0.81	0.87	0.96	1.11
HDE 242935 A	05:22:46.54	+33:25:11.5	O6.5 V((f))z	S11a	0.49	0.83	0.92	1.12
HD 35619	05:27:36.15	+34:45:19.0	O7.5 V((f))	MA16	0.73	0.64	0.71	0.97
HD 36879	05:35:40.53	+21:24:11.7	O7 V(n)((f))	MA16	0.60	0.76	0.72	0.95
HD 41161	06:05:52.46	+48:14:57.4	O8 Vn	S11	0.98	0.87	0.78	0.80
HD 41997	06:08:55.82	+15:42:18.2	O7.5 Vn((f))	S11	0.71	0.77	0.55	0.72
HD 42088	06:09:39.57	+20:29:15.5	O6 V((f))z	S11	0.63	0.81	1.06	1.30
HD 44811	06:24:38.35	+19:42:15.8	O7 V(n)z	S11	0.70	0.75	0.95	1.27
ALS 19265	06:24:59.85	+26:49:20.0	O4.5 V((c))z	MA16	0.31	1.10	1.24	1.13

Table 1—Continued

HDE 256725 A	06:25:01.30	+19:50:56.1	O5 V((fc))	MA16	0.34	0.94	0.92	0.97
HD 46056 A	06:31:20.86	+04:50:03.9	O8 Vn	S11	0.80	0.69	0.75	0.94
HD 46150	06:31:55.52	+04:56:34.3	O5 V((f))z	S11	0.26	0.57	0.79	1.39
HD 46573	06:32:09.31	+04:49:24.7	O4 V((f))	S11	0.16	0.70	0.70	0.99
HD 46485	06:33:50.96	+04:31:31.6	O7 V((f))n var?	MA16	0.80	0.78	0.82	1.03
Tyc 0737-01170-1	06:36:29.00	+10:49:20.7	O7 Vz	MA16	0.61	0.77	0.98	1.27
HD 48279 A	06:42:40.55	+01:42:58.2	O8.5 V Nstr var?	MA16	0.98	0.90	0.96	0.98
ALS 207	07:09:55.20	-18:30:07.9	O6.5 V((f))	MA16	0.57	0.91	0.98	1.08
HD 57236	07:19:30.10	-22:00:17.3	O8.5 V	S14	0.83	0.59	0.85	1.03
ALS 458	07:30:01.27	-19:08:35.0	O6.5 V((f))z	MA16	0.59	0.80	0.91	1.14
BD -15 1909	07:34:58.46	-16:14:23.2	O6.5 V((f))z	MA16	0.61	0.81	0.93	1.15
CPD -26 2704	07:52:36.52	-26:22:42.0	O7 V(n)	MA16	0.78	0.89	0.88	0.99
HD 64568	07:53:38.21	-26:14:02.6	O3 V((f*))z	S14	0.00	0.78	0.95	1.23
CPD -47 2962	08:57:51.66	-47:45:43.9	O7 V((f))	MA16	0.64	0.95	0.86	0.91
CPD -49 2322	09:15:52.79	-50:00:43.8	O7.5 V((f))	MA16	0.69	0.56	0.68	0.99
HDE 298429	09:30:37.25	-51:39:34.7	O8.5 V	S14	0.92	0.60	0.73	0.80
2MASS J10224096-5930305	10:22:40.96	-59:30:30.6	O7 V((f))z	MA16	0.55	0.58	0.74	1.27
2MASS J10224377-5930182	10:22:43.77	-59:30:18.2	O8 V(n)	MA16	0.75	0.50	0.61	0.81
HD 90273	10:23:44.45	-57:38:31.5	ON7 V((f))	MA16	0.68	0.85	0.87	1.03
HD 91837	10:34:49.51	-60:11:14.1	O8.5 Vn	S14	0.84	0.62	0.72	0.86
HD 92206+B	10:37:22.96	-58:37:23.0	O6 V((f))	MA16	0.48	0.75	0.81	1.08
HD 92504	10:39:36.87	-57:27:40.7	O8.5 V(n)	S14	0.83	0.58	0.80	0.96
HDE 305438	10:42:43.77	-59:54:16.5	O8 Vz	S14	0.73	0.89	0.98	1.10
HDE 303316 A	10:43:11.18	-59:44:21.0	O7 V((f))z	S14	0.52	0.64	0.90	1.42
CPD -58 2611	10:43:46.69	-59:32:54.8	O6 V((f))z	S14	0.45	0.71	0.92	1.29
HD 93128	10:43:54.37	-59:32:57.4	O3.5 V((fc))z	S14	0.08	0.68	0.79	1.16
Trumpler 14-9	10:43:55.35	-59:32:48.6	O8.5 V	S14	0.85	0.67	0.87	1.03
HD 93129 B	10:43:57.64	-59:32:53.5	O3.5 V((f))z	MA16	0.13	0.74	0.83	1.12
CPD -58 2620	10:43:59.92	-59:32:25.4	O7 V((f))z	S14	0.59	0.66	0.96	1.46
HD 93204	10:44:32.34	-59:44:31.0	O5.5 V((f))	S14	0.33	0.81	0.65	0.80
HDE 303311	10:44:37.46	-59:32:55.4	O6 V((f))z	S14	0.41	0.78	1.02	1.31

Table 1—Continued

HDE 305524	10:44:45.24	-59:54:41.6	O6.5 Vn((f))z	S14	0.57	0.67	0.83	1.23
CPD -59 2610	10:44:54.71	-59:56:01.9	O8.5 V	S14	0.81	0.78	0.84	1.04
[ARV2008] 206	10:45:22.28	-59:50:47.1	O6 V((f))	S14	0.40	0.68	0.66	0.98
HDE 305532	10:45:34.07	-59:57:26.7	O6.5 V((f))z	S14	0.49	0.72	0.95	1.32
CPD -59 2673	10:46:22.46	-59:53:20.5	O5.5 V(n)((f))z	S14	0.40	0.76	0.92	1.21
HDE 305539	10:46:33.07	-60:04:12.6	O8 Vz	S14	0.79	0.73	0.89	1.13
HDE 305612	10:47:16.42	-60:05:40.0	O8 V(n)z	S14	0.75	0.68	0.83	1.11
HD 96715	11:07:32.82	-59:57:48.7	O4 V((f))z	S14	0.21	0.67	0.94	1.40
HD 97848	11:14:31.90	-59:01:28.8	O8 V	S14	0.82	0.67	0.76	0.92
NGC 3603 HST-51	11:15:07.50	-61:15:46.3	O5.5 V(n)	MA16	0.22	0.64	0.52	0.81
NGC 3603 MTT 25	11:15:11.32	-61:15:55.6	O5 V(n)	MA16	0.23	0.66	0.49	0.74
HD 97966	11:15:11.78	-59:24:58.3	O7 V((f))z	MA16	0.54	0.61	0.86	1.40
HD 99546	11:26:36.90	-59:26:13.6	O7.5 V((f)) Nstr	MA16	0.72	0.82	0.78	0.95
HD 101223	11:38:22.77	-63:12:02.8	O8 V	S14	0.78	0.51	0.72	0.92
HD 110360	12:42:12.70	-60:39:08.7	ON7 V	MA16	0.74	1.02	1.06	1.04
CPD -61 3973	13:45:21.10	-62:25:35.4	O7.5 V((f))	MA16	0.76	0.79	0.84	1.06
HD 122313	14:03:12.99	-62:15:38.6	O8.5 V	MA16	0.91	0.56	0.85	0.93
HD 144647	16:09:16.20	-49:36:21.8	O8.5 V(n)	MA16	0.88	0.63	0.81	0.91
HDE 329100 A	16:54:42.30	-45:15:14.8	O8 V(n)	MA16	0.79	0.62	0.64	0.81
HDE 326775	17:05:31.31	-41:31:20.1	O6.5 V(n)((f))z	MA16	0.48	0.69	0.80	1.16
ALS 18770	17:19:00.80	-38:49:23.1	O7 V((f))	MA16	0.55	0.75	0.76	1.01
ALS 18768	17:19:01.05	-38:48:58.9	O8.5 V	S14	1.03	0.52	1.00	0.97
Pismis 24-15	17:24:28.95	-34:14:50.7	O7.5 Vz	MA16	0.83	0.66	0.93	1.12
ALS 17696	17:24:42.33	-34:13:21.4	O7.5 V	S14	0.76	1.13	0.87	0.77
Pismis 24-2	17:24:43.31	-34:12:44.2	O5 V((f))	S14	0.31	0.74	0.80	1.08
ALS 16052	17:24:45.78	-34:09:39.9	O6 V((f))z	S14	0.48	0.65	0.87	1.34
HD 164492 A	18:02:23.55	-23:01:51.1	O7.5 Vz	S14	0.66	0.82	1.05	1.27
ALS 4626	18:04:17.88	-13:06:13.7	ON6 V((f))	MA16	0.50	1.13	1.11	0.98
HD 167633	18:16:49.66	-16:31:04.3	O6.5 V((f))	S11	0.48	0.86	0.80	0.93
ALS 4880	18:17:33.67	-12:05:42.8	O6 V((f))	MA16	0.47	0.72	0.76	1.05
ALS 15360	18:18:37.48	-13:43:39.2	O7 V((f))z	MA16	0.50	0.80	0.90	1.13

Table 1—Continued

HD 168461	18:20:17.18	-12:10:19.2	O7.5V((f))Nstr	MA16	0.72	0.84	0.77	0.92
HD 168504	18:20:34.10	-13:57:15.7	O7.5V(n)z	MA16	0.71	0.75	0.88	1.18
ALS 19618	18:20:34.50	-16:10:11.7	O4V(n)((fc))	MA16	0.18	0.78	0.75	0.96
BD -14 5014	18:22:22.31	-14:37:08.5	O7.5V(n)((f))	MA16	0.55	0.50	0.58	1.06
BD -10 4682	18:24:20.65	-10:48:34.3	O7Vn((f))	MA16	0.66	0.90	0.82	0.90
BD -14 5040	18:25:38.90	-14:45:05.7	O5.5V(n)((f))	MA16	0.38	0.77	0.83	1.07
BD -04 4503	18:35:32.54	-04:47:55.4	O7V	MA16	0.79	0.95	0.92	0.97
HDE 344758	19:41:52.72	+24:20:51.1	O8.5V(n)((f))	MA16	0.83	0.69	0.70	0.84
HDE 344777	19:42:11.47	+23:26:00.5	O7.5Vz	MA16	0.69	0.70	0.79	1.12
HDE 344784 A	19:43:10.97	+23:17:45.4	O6.5V((f))z	MA16	0.48	0.58	0.69	1.18
HDE 338916	19:45:42.12	+25:21:16.4	O7.5Vz	MA16	0.73	0.84	0.95	1.13
HDE 227018	19:59:49.10	+35:18:33.5	O6.5V((f))z	MA16	0.47	0.69	0.87	1.26
HDE 227245	20:02:21.71	+35:40:29.8	O7V((f))z	MA16	0.56	0.66	0.87	1.32
HDE 227465	20:04:27.22	+33:42:18.4	O7V((f))	MA16	0.66	0.68	0.64	0.94
HD 191978	20:10:58.28	+41:21:09.9	O8V	MA16	0.80	0.54	0.82	1.03
HDE 228759	20:17:07.54	+41:57:26.5	O6.5V(n)((f))z	MA16	0.53	0.67	0.80	1.20
ALS 18707	20:17:41.93	+36:45:25.6	O6.5V((f))z	MA16	0.44	0.70	0.79	1.13
HDE 228841	20:18:29.69	+38:52:39.8	O6.5Vn((f))	S11	0.60	0.89	0.83	0.93
HD 193595	20:19:31.33	+39:03:26.2	O7V((f))	MA16	0.66	0.92	0.99	1.08
HDE 229202	20:23:22.84	+40:09:22.5	O7.5V(n)((f))	MA16	0.65	0.64	0.66	1.01
ALS 11355	20:27:17.57	+39:44:32.6	O8V(n)((f))	MA16	0.75	0.59	0.71	0.95
BD +40 4179	20:27:43.62	+40:35:43.5	O8Vz	MA16	0.70	0.72	0.81	1.12
2MASS J20315961+4114504	20:31:59.61	+41:14:50.5	O7.5Vz	MA16	0.62	0.81	0.96	1.18
Cyg OB2-6	20:32:45.45	+41:25:37.5	O8.5V(n)	MA16	0.79	0.61	0.71	0.91
ALS 15111	20:32:59.13	+41:24:25.0	O8V	MA16	0.82	0.59	0.83	1.01
Cyg OB2-22 B	20:33:08.83	+41:13:17.4	O6V((f))	S11	0.43	0.66	0.56	0.85
Cyg OB2-8 D	20:33:16.33	+41:19:02.0	O8.5V(n)	S14	0.75	0.46	0.76	1.02
Cyg OB2-24	20:33:17.48	+41:17:09.3	O8V(n)	S11	0.71	0.74	0.68	0.92
Cyg OB2-25 A	20:33:25.54	+41:33:26.7	O8Vz	MA16	0.69	0.59	0.82	1.19
ALS 15134	20:33:26.76	+41:10:59.5	O8Vz	MA16	0.76	0.67	0.87	1.15
BD +45 3216 A	20:33:50.37	+45:39:40.9	O5V((f))z	MA16	0.38	0.86	1.08	1.26

Table 1—Continued

BD +36 4145	20:36:18.21	+37:25:02.8	O8.5 V(n)	MA16	0.78	0.71	0.72	0.92
ALS 12050	21:55:15.29	+57:39:45.7	O5 V((f))	MA16	0.25	0.74	0.64	0.86
BD +55 2722 A	22:18:58.63	+56:07:23.5	O8 Vz	MA16	0.73	0.72	0.84	1.14
ALS 12370	22:23:17.42	+55:38:02.3	O6.5 Vnn((f))	MA16	0.61	0.92	0.89	0.97
HD 213023 A	22:26:52.36	+63:43:04.9	O7.5 Vz	MA16	0.69	0.72	0.86	1.20
ALS 12619	22:47:50.60	+58:05:12.4	O7 V((f))z	MA16	0.71	0.81	1.10	1.36
HD 216532	22:52:30.56	+62:26:25.9	O8.5 V(n)	S11	0.93	0.69	0.77	0.83
BD +55 2840	22:55:08.49	+56:22:58.9	O7.5 V(n)	MA16	0.72	0.79	0.76	0.96
HD 217086	22:56:47.19	+62:43:37.6	O7 Vnn((f))z	S14	0.61	0.69	0.83	1.20
BD +60 2635	23:53:05.21	+60:54:44.6	O6 V((f))	MA16	0.48	0.91	0.95	1.04

Table 2. O binaries with single-lined profiles at the GOSSS resolution

Object	R.A. hh:mm:ss.ss	Decl. dd:am:as.s	Sp. Type	Ref.	EW(He I 4471) [Å]	EW(He II 4542) [Å]	EW(He II 4686) [Å]	z
V747 Cep	00:01:46.87	+67:30:25.1	O5.5V(n)((f))	MA16	0.39	0.70	0.66	0.94
HD 14633 AaAb	02:22:54.29	+41:28:47.7	ON8.5V	S11	1.01	0.78	0.72	0.71
HD 17520 A	02:51:14.43	+60:23:10.0	O8 V	MA16	0.80	0.75	0.68	0.85
HDE 242908	05:22:29.30	+33:30:50.4	O4.5V(n)((fc))z	S14	0.28	0.74	0.94	1.26
HD 46149	06:31:52.53	+05:01:59.2	O8.5V	S11
HD 46573	06:34:23.57	+02:32:02.9	O7V((f))z	S11	0.72	0.77	0.88	1.15
15 Mon AaAb	06:40:58.66	+09:53:44.7	O7V((f))z var	S14	0.70	0.67	0.78	1.12
ALS 85	06:45:48.84	-07:18:46.4	O7.5V	MA16	0.69	0.86	0.89	1.04
HD 53975	07:06:35.96	-12:23:38.2	O7.5Vz	S11	0.75	0.70	0.83	1.11
HD 54662 AB	07:09:20.25	-10:20:47.6	O7 Vz var?	S14
V467 Vel	08:43:49.81	-46:07:08.8	O6.5V(n)((f))	MA16	0.51	0.62	0.52	0.83
HD 91572	10:33:12.27	-58:10:13.6	O6.5V((f))z	S14	0.50	0.61	0.74	1.22
HD 91824	10:34:46.63	-58:09:22.0	O7V((f))z	S14	0.60	0.78	0.89	1.14
HD 92206 A	10:37:22.28	-58:37:22.8	O6V((f))z	S14
HD 93146 A	10:44:00.16	-60:05:09.9	O7V((f))	MA16	0.68	0.79	0.78	0.98
HD 93222 AB	10:44:36.25	-60:05:28.9	O7V((f))	MA16	0.62	0.66	0.72	1.09
CPD -59 2600	10:44:41.79	-59:46:56.4	O6V((f))	S14	0.40	0.69	0.65	0.94
CPD -59 2626 AB	10:45:05.79	-59:45:19.6	O7.5V(n)	MA16	0.73	0.78	0.72	0.92
HDE 303308 AB	10:45:05.92	-59:40:05.9	O4.5V((fc))	S14	0.23	0.64	0.55	0.86
CPD -59 2641	10:45:16.52	-59:43:37.0	O6V((fc))	S14	0.33	0.63	0.55	0.87
HD 101191	11:38:12.17	-63:23:26.8	O8 V	S14	0.74	0.50	0.76	1.03
HD 101413 AB	11:39:45.84	-63:28:40.1	O8 V	S14	0.76	0.63	0.65	0.85
HD 101436	11:39:49.96	-63:28:43.6	O6.5V((f))	S14
HD 123590 AB	14:10:43.97	-62:28:44.4	O8 V	S14
HD 145217	16:12:00.30	-50:18:20.5	O8 V	MA16
HD 150135 AaAb	16:41:19.45	-48:45:47.5	O6.5V((f))z	S14
HD 152590	16:56:05.22	-40:20:57.6	O7.5Vz	S14	0.68	0.71	0.90	1.27
HD 152623 AaAbB	16:56:15.03	-40:39:35.8	O7V(n)((f))	MA16
HD 155913	17:16:26.34	-42:40:04.1	O4.5Vn((f))	S14	0.31	0.86	0.75	0.88

Table 2—Continued

HDE 319699	17:19:30.42	-35:42:36.1	O5 V((fc))	S14	0.25	0.73	0.57	0.79
HDE 319703 BaBb	17:19:45.05	-36:05:47.0	O6 V((f))z	S14	0.47	0.60	0.71	1.19
ALS 19693	17:25:29.17	-34:25:15.7	O6 Vn((f))	MA16	0.38	0.76	0.74	0.97
HD 164536	18:02:38.62	-24:15:19.4	O7.5 V(n)	MA16	0.75	0.71	0.81	1.07
9 Sgr AB	18:03:52.45	-24:21:38.6	O4 V((f))	MA16
HD 165246	18:06:04.68	-24:11:43.9	O8 V(n)	S14	0.81	0.59	0.75	0.93
HD 168075	18:18:36.04	-13:47:36.5	O7 V((f))	MA16
HD 168137 AaAb	18:18:56.19	-13:48:31.1	O8 Vz	MA16	0.72	0.72	0.88	1.22
BD -16 4826	18:21:02.23	-16:01:00.9	O5.5 V((f))z	MA16	0.42	0.69	0.84	1.21
V479 Sct	18:26:15.05	-14:50:54.3	ON6 V((f))z	MA16	0.51	0.94	1.05	1.12
Cyg OB2-17	20:32:50.01	+41:23:44.7	O8 V	MA16	0.77	0.80	0.80	1.00
ALS 15115	20:33:18.05	+41:21:36.9	O8 V	MA16
Cyg OB2-29	20:34:13.50	+41:35:03.0	O7.5 V(n)((f))z	MA16	0.62	0.62	0.79	1.27
ALS 15114	20:34:29.60	+41:31:45.4	O7.5 V(n)((f))	MA16
HD 199579	20:56:34.78	+44:55:29.0	O6.5 V((f))z	S11	0.57	0.60	0.85	1.40
BD +62 2078	22:25:33.58	+63:25:02.6	O7 V((f))z	MA16	0.62	0.82	0.92	1.13

Table 3. Double-lined binary stars in GOSSS

Object	R.A. hh:mm:ss.ss	Decl. dd:mm:ss	Sp. Classif. Prim. + Second.	Ref.	EW(He I 4471) [Å]		EW(He II 4542) [Å]		EW(He II 4686) [Å]		z
					Prim./Second.	Prim./Second.	Prim./Second.	Prim./Second.	Prim./Second.		
ALS 6967	02:12:29.97	+59:54:04.1	O8 V + B0: V	MA16	0.63	0.38	0.52	0.83	0.83
BD +60 497	02:31:57.09	+61:36:43.9	O6.5 V(f) + O8/B0 V	S11
HD 18326	02:59:23.17	+60:33:59.5	O6.5 V(f)z + O9/B0 V:	S14
MY Cam	03:59:18.29	+57:14:13.7	O5.5 V(n) + O6.5 V(n)	MA16	0.23/0.29	0.78/0.36	0.51/0.38	0.65/1.06	0.65/1.06
ALS 8272	05:20:00.63	+38:54:43.5	O7 V(f) + B0 III-V	MA16	0.44	0.58	0.53	0.92	0.92
HD 48099	06:41:59.23	+06:20:43.5	O5.5 V(f)z + O9 V	MA16
HD 64315 AB	07:52:20.28	-26:25:46.7	O5.5 V + O7 V	MA16	0.34/0.37	0.61/0.41	0.63/0.35	1.03/0.84	1.03/0.84
HD 92206 C	10:37:18.63	-58:37:41.7	O8 V(n)z + B0: V	MA16	0.46	0.45	0.53	1.17	1.17
ALS 15204	10:43:41.24	-59:35:48.2	O7.5 Vz + O9: V	MA16
HD 93161 A *	10:44:08.84	-59:34:34.5	O7.5 V + O9 V	S14	0.42	0.60	0.67	1.11	1.11
HD 93205	10:44:33.74	-59:44:15.5	O3.5 V(f) + O8 V	S14
CPD -59 2591	10:44:36.69	-59:47:29.6	O8 Vz + B0.5: V:	MA16	0.58	0.58	0.69	1.19	1.19
V572 Car	10:44:47.31	-59:43:53.2	O7.5 V(n) + B0 V(n)	MA16	0.63	0.44	0.57	0.91	0.91
HD 93343	10:45:12.22	-59:45:00.4	O8 V + sec	MA16
CPD -59 2635	10:45:12.72	-59:44:46.2	O8 V(n) + O9.5 V	S14	0.57	0.55	0.42	0.72	0.72
CPD -59 2636 AB	10:45:12.87	-59:44:19.2	O8 V + O8 V	S14
V662 Car	10:45:36.32	-59:48:23.2	O5 V(n)z + B0: V	MA16	0.24	0.77	0.85	1.11	1.11
HDE 305525	10:46:05.70	-59:50:49.4	O5 V(n)z + B0: V	MA16
ALS 18551 *	10:58:17.68	-61:12:03.5	O5.5 V(n)((f))z + sec	S14
2MASS J10583238-6110565	10:58:32.39	-61:10:56.5	O4.5 V(n)z + O4.5 V(n)z	MA16	0.11/0.07	0.47/0.45	0.44/0.38	0.93/0.85	0.93/0.85
HD 97484	11:12:04.50	-61:05:42.9	O5 V(f) + O7 V(f)	MA16
HD 100213	11:31:10.93	-65:44:32.1	O7.5 V(f) + O7.5 V(f)	MA16	0.37/0.34	0.46/0.33	0.34/0.27	0.74/0.79	0.74/0.79
HD 101131 AB	11:37:48.44	-63:19:23.5	O8 V(n) + B0 V(n)	MA16	0.54	0.45	0.53	0.98	0.98
Tyc 7370-00460-1	17:18:15.40	-34:00:05.9	O5.5 V(f) + O8: V	S14
HDE 319703 A	17:19:46.16	-36:05:52.4	O6 V(f) + O8 V	MA16	0.33/0.22	0.41/0.37	0.43/0.38	1.04/1.03	1.04/1.03
HD 159176	17:34:42.49	-32:34:54.0	O7 V(f) + O9.5 V	MA16
HD 161853	17:49:16.56	-31:15:18.1	O7 V(f) + O7 V(f)	S14	0.34/0.42	0.39/0.38	0.36/0.32	0.94/0.75	0.94/0.75
Herschel 36	18:03:40.33	-24:22:42.7	O8 V(n)z + B	S14	0.66	0.52	0.80	1.20	1.20
HD 165052	18:05:10.55	-24:23:54.8	O7: V + sec	S14
HD 165921	18:09:17.70	-23:59:18.3	O6 Vz + O8 Vz	MA16
ALS 4923	18:19:28.43	-15:18:46.2	O7 V(n)z + B0: V:	S14	0.42	0.69	0.72	1.04	1.04
HD 175514	18:55:23.12	+09:20:48.1	O8.5 V + O8.5 V	MA16	0.36/0.33	0.32/0.32	0.39/0.28	1.09/0.84	1.09/0.84
HD 194649 AB	20:25:22.12	+40:13:01.1	O7 V(n)((f))z + B	MA16
Cyg OB2-73	20:34:21.93	+41:17:01.6	O6.5 V(f) + sec	MA16
HD 206267 AaAb	21:38:57.62	+57:29:20.6	O8 Vz + O8 Vz	MA16	0.39/0.28	0.27/0.27	0.49/0.32	1.26/1.14	1.26/1.14
			O6.5 V(f) + O9/B0 V	S11a	0.52	0.75	0.53	0.71	0.71

Table 3—Continued

BD +55 2722 C	22:18:59.88	+56:07:18.9	O7 V(n)z + B	MA16	0.51	0.72	0.80	1.11
HD 215835	22:46:54.11	+58:05:03.5	O5.5 V((f)) + O6 V((f))	S14	0.13/0.37	0.50/0.40	0.41/0.38	0.81/0.96
ALS 12688	22:55:44.94	+56:28:36.7	O5.5 V(n)((fe)) + B	MA16	0.35	0.64	0.50	0.79

Table 4. Clusters and H II regions containing O Vz stars

Nebular Complex/Association	Cluster/H II region	O Vz	Stars	O V non-z	
NGC 3372/Car OB1	Trumpler 14	4	CPD -58 2611 , HD 93128, HD 93129 B, CPD -58 2620	1	
	Trumpler 16	5	HDE 303311 , CPD -59 2591, HD 93161A, V662Car, HDE 303316 A	7	
	Collinder 228	4	HDE 305524 , HD 305438, HDE 305532 , CPD -59 2673	1	
	Bochum 11	2	HDE 305539, HDE 305612	0	
	NGC 3324	1	HD 92206 C	1	
	NGC 3293	2	HD 91824 HD 91572	0	
	...	1	2MASS J10224096-5930305	2	
	Cygnus X	Sh 2-109	12	Cyg OB2-29 , Cyg OB2-25A, ALS 15134, BD +45 3216 A , HDE 228759 , HDE 227018 , HDE 227245 , HD 199579 ALS 18 707, 2MASS J20315961+4114504, Schulte 73 (both components)	9
	Cyg OB9	Sh 2-108	1	BD +40 4179	4
	“Heart and Soul” Nebula	IC 1795, IC 1805, IC 1848	3	BD +61 411 A , BD +60 501 , BD +60 586 A	4
Ser OB1	NGC 6611/M16	3	HD 168137 AaAb , HD 168504, ALS 15360	0	
	NGC 6618/M17	1	BD -16 4826	1	
Sct OB3	Sh 2-50	1	V479 Sct	1	
Cepheus/Cep OB1, Cep OB2 Cep OB3, Cep OB4	Sh 2-145	2	BD +62 2078, HD 213023 A	0	
	Teutsch 127	2	BD +55 2722 A, BD +55 2722 C	1	
	NGC 7380	1	ALS 12619	1	
	Sh 2-155	1	HD 217086	1	
NGC 6357	Berkeley 59	2	BD +66 1675 , Tyc 4026-00424-1	1	
	Pismis 24	2	ALS 16052 , Pismis 24-15	4	
	NGC 6334	1	HDE 319703 BaBb	1	
	Mon OB1	2	Tyc 0737-01170-1 , 15 Mon AaAb	0	
Rosette Nebula/Mon OB2	NGC 2244	1	HD 46150	3	
	Sh 2-280	1	HD 46573	0	

Table 4—Continued

Gem OB1	NGC 2175	1	HD 42088	0
Pup OB1	NGC 2467	1	HD 64568	2
Sgr OB1	NGC 6514	1	HD 164492 A	0
Sgr OB5	Sh 2-15	1	HD 161 853	0
Vul OB1,Vul OB4	NGC 6823	2	HDE 344784 A, HDE 344777	0
	Sh 2-88	1	HDE 338916	0
Aur OB2,Aur OB1	NGC 1893	5	ALS 8294, BD +33 1025 A, HDE 242908 , HDE 242926, HDE 242935 A	0
CMa OB1	IC 2177,Sh 2-296	1	HD 53975	0
Cam OB1,Per OB3,Cam OB3	Alicante 1	1	ALS 7833	1
Sco OB1	Trumpler 24	1	HD 152590	0
Cas OB7	Sh 2-180	1	ALS 6351	0
Collinder 121	Sh 2-306	1	ALS 458	0
	...	1	BD -15 1909	0
...	RCW 113	1	HDE 326 775	1
...	RCW 54	1	HD 96715	2
...	...	3	HD 44811, HD 97966, HD 19265	12

Table 5. Clusters containing O V stars but not Vz objects

Nebular Complex/Association	Cluster/H II region	O V	Stars
...	Pismis 11	1	CPD -49 2322
...	Bochum 1	1	HDE 256725 A
Car OB1	Bochum 9	1	HD 91837
Sgr OB1	Collinder 367	1	HD 165921
...	Havlen-Moffat 1	2	ALS 18770, ALS 18768
...	IC 1590	2	HD 5005 A, HD 5005 C
Cru OB1	IC 2944	3	HD 101191, HD 101223, HD 101413 AB
Sgr OB1	IC 4701	1	HD 167633
...	NGC 6383	1	HD 159176
Ser OB2	NGC 6604	2	ALS 4880, HD 168461
...	RCW 114	1	HD 155913
Ser OB1	RCW 161	1	ALS 4923
...	RCW 167	1	BD -10 4682
...	Sh 2-10	1	Tyc 7370-00460-1
Cas OB7, Cas OB1	Sh 2-185	1	BD +60 134
Cas OB 6	...	1	BD +62 424
Aur OB1	Sh 2-227	1	ALS 8272
Aur OB2, Aur OB1	Sh 2-230	1	HD 35619
...	Sh 2-289	1	LS 85
Ser OB1	Sh 1-48	1	BD -14 5014
Cep OB2	Trumpler 37	1	HD 206267 AaAb
Vel OB1, Vel OB2	...	1	V467 Vel
Cas OB5	...	1	BD +60 2635
...	...	1	BD +55 2840
Cep OB2	...	1	ALS 12050
Vul OB1, Vul OB4	...	1	HDE 344758
Cen OB1	...	1	HD 110360

We thank the anonymous referee for useful suggestions and comments on the manuscript. We also thank the staff of Las Campanas Observatory for their support during the observing runs. J.I.A and R.H.B acknowledge financial support from the Chilean Government grants, through the FONDECYT Iniciación 11121550 and FONDECYT Regular 1140076 projects, respectively. S.S.-D. acknowledges financial support from the Spanish Ministry of Economy and Competitiveness (MINECO) under grants AYA2010-21697-C05-04, and Severo Ochoa SEV-2011-0187, and by the Canary Islands Government under grant PID2010119. J.M.A., A.S., and E.J.A. acknowledge support from [a] the Spanish Government Ministerio de Economía y Competitividad (MINECO) through grants AYA2010-15 081, AYA2010-17 631, and AYA2013-40 611-P and [b] the Consejería de Educación of the Junta de Andalucía through grant P08-TIC-4075. C.S.-S. acknowledges support from the Joint Committee ESO-Government of Chile. I.N. and A.M. acknowledge support from the Spanish Ministerio de Ciencia e Innovación (MICINN) under grant AYA2012-39364-C02-02, and by the Generalitat Valenciana (ACOMP/2014/129). A.M. acknowledges support from the Generalitat Valenciana through the grant BEST/2015/242. The Space Telescope Science Institute is operated by the Association of Universities for Research in Astronomy, Inc., under NASA contract NAS5- 26555. This research has made use of Aladin (Bonnarel et al. 2000), and the SIMBAD database, operated at CDS, Strasbourg, France.

REFERENCES

- Barbá, R. H., Gamen, R. C., Arias, J. I., et al. 2010, *RMxAC*, 38, 30
- Bonnarel, F., Fernique, P., Bienaymé, O., et al. 2000, *A&A*, 143, 33
- Conti, P. S.; Alschuler, W. R. 1971, *ApJ*, 170, 3
- Conti, P. S.; Leep, E. M. 1974, *ApJ*, 193, 113
- Evans, C. J., Taylor, W. D., Hénault-Brunet, V., et al. 2011, *A&A*, 530, A108
- Finkbeiner, D. P. 2004, *ApJ*, 614, 186
- Havlen, R. J., & Moffat, A. F. J., 1977, *A&A*, 58, 351
- Kharchenko, N. V., Piskunov, A. E., Schilbach, E., et al. 2013, *A&A*, 558A, 53
- Koenig, X. P., Leisawitz, D. T., Benford, D. J., et al. 2012, *ApJ*, 744, 130

- Lorenzo, J., Simón-Díaz, S., Negueruela, I., Vilardell, F. 2010, in ASP Conf. Ser. 435, BinariesKey to Comprehension of the Universe, ed. A. Prsa, M. Zejda (San Francisco: ASP), 409
- Maíz Apellániz, J., Sota, A., Walborn, N. R., et al. 2011, Highlights of Spanish Astrophysics VI, Proc. of the IX Scientific Meeting of the Spanish Astronomical Society (SEA), held in Madrid, Eds.: M. R. Zapatero Osorio, J. Gorgas, J. Maíz Apellániz, J. R. Pardo, and A. Gil de Paz., 467
- Maíz Apellániz, J., Walborn, N. R., Galué, H. A., et al. 2004, ApJS, 151, 103
- Maíz Apellániz, J., Alfaro, E. J., Arias, J. I., et al. 2015, Highlights of Spanish Astrophysics VIII, Proc. of the XI Scientific Meeting of the Spanish Astronomical Society held in Teruel, Spain, ISBN 978-84-606-8760-3. A. J. Cenarro, F. Figueras, C. Hernandez-Monteagudo, J. Trujillo Bueno, and L. Valdivielso (eds.), 603
- Maíz Apellániz, J., Sota, A., Arias, J. I., et al. 2016, submitted
- Markova, N., Puls, J., Scuderi, S., et al. 2011, A&A, 530, 11
- Martins, F., Schaerer, D., Hillier, D. J. 2005, A&A, 436, 1049
- Mason, B. D., Hartkopf, W. I., Gies, D. R., et al. 2009, AJ, 137, 3358
- Mathys, G. 1988, A&AS, 76, 427
- Mathys, G. 1989, A&AS, 81, 237
- McSwain, M. V., & Gies, D. R. 2005, ApJS, 161, 118
- Parker, J. W., Garmany, C. D., Massey, P., Walborn, N. R. 1992, AJ, 103, 1205
- Penny, L. R., Gies, D. R., Hartkopf, W. I., et al. 1993 PASP, 105, 588
- Puls, J., Urbaneja, M. A., Venero, R., et al. 2005, A&A, 435, 669
- Rochau, B., Brandner, W., Stolte, A., et al. 2011, MNRAS, 418, 949
- Sabín-Sanjulián, C., Simón-Díaz, S., Herrero, A., et al. 2014, A&A, 564, A39
- Sana, H., de Koter, A., de Mink, S. E., et al. 2013, A&A, 550A, 107
- Sana, H., Le Bouquin, J.-B.; Lacour, S., et al. 2014, ApJS, 215, 15
- Santolaya-Rey, A. E., Puls, J.; Herrero, A. 1997, A&A, 323, 488

- Simón-Díaz, S., Castro, N., García, M., et al. 2011, Active OB stars: structure, evolution, mass loss, and critical limits, Proc. of the International Astronomical Union, IAU Symposium, 272, 310
- Simón-Díaz, S., Castro, N., Herrero, A., et al. 2011, Journal of Physics: Conference Series, 328, Issue 1, id. 012021
- Simón-Díaz, S., Herrero, A., Sabín-Sanjulián, C., et al. 2014, A&A, 570L, 6
- Simón-Díaz, S., Negueruela, I., Maíz Apellániz, J., et al. 2015, Highlights of Spanish Astrophysics VIII, Proc. of the XI Scientific Meeting of the Spanish Astronomical Society held in Teruel, Spain, ISBN 978-84-606-8760-3. A. J. Cenarro, F. Figueras, C. Hernández-Monteagudo, J. Trujillo Bueno, and L. Valdivielso (eds.), 576
- Sota, A., Maíz Apellániz, J., Walborn, N. R., et al. 2011, ApJS, 193, 24
- Sota, A., Maíz Apellániz, J., Morrell, N. I., et al. 2014, ApJS, 211, 10
- Tokovinin, A., Mason, B. D., Hartkopf, W. I. 2010, AJ, 139, 743
- Walborn, N. R. 1973, ApJ, 179, 517
- Walborn, N. R., Fitzpatrick, E. L. 1990, PASP, 102, 379
- Walborn, N. R., Parker, J. W. 1992, ApJ, 399L, 87
- Walborn N. R., Blades J.C. 1997, ApJS, 112, 457
- Walborn, N. R., Barbá, R. H., Brandner, W., et al. 1999, AJ, 117, 225
- Walborn, N. R. 2001, ASPC, 242, 217
- Walborn, N. R. 2009, Massive Stars: From Pop III and GRBs to the Milky Way. Space Telescope Science Institute Symposium Series No. 20. Eds. Mario Livio and Eva Villaver. Cambridge University Press, 2009, ISSN 9780521762632, 167
- Walborn, N. R. 2010, ASPC, 425, 45
- Walborn, N. R., Sota, A., Maíz Apellániz, J., et al. 2010, ApJ, 711, L143
- Walborn, N. R., Maíz Apellániz, J., Sota A., et al. 2011, AJ; 142, 150
- Walborn, N. R., Sana, H., Simón-Díaz, S., et al. 2014, A&A, 564, A40
- Wolk, S. J., Broos, P. S., Getman, K. V., et al. 2011, ApJS, 194, 12

